Acta Oceanol. Sin., 2021, Vol. 40, No. 1, P. 85–102
https://doi.org/10.1007/s13131-021-1705-6
http://www.hyxb.org.cn
E-mail: hyxbe@263.net

An evaluation of the Arctic clouds and surface radiative fluxes in CMIP6 models

Jianfen Wei[1, 2], Zhaomin Wang[3, 4*], Mingyi Gu[5], Jing-Jia Luo[2, 6*], Yunhe Wang[7, 8]

[1] School of Environmental Science and Engineering, Nanjing University of Information Science and Technology, Nanjing 210044, China

[2] Institute for Climate and Application Research (ICAR), Nanjing University of Information Science and Technology, Nanjing 210044, China

[3] College of Oceanography, Hohai University, Nanjing 210098, China

[4] Southern Marine Science and Engineering Guangdong Laboratory (Zhuhai), Zhuhai 519082, China

[5] School of Atmospheric Science, Nanjing University of Information Science and Technology, Nanjing 210044, China

[6] Key Laboratory of Meteorological Disaster of Ministry of Education/Joint International Research Laboratory of Climate and Environment Change/Collaborative Innovation Center on Forecast and Evaluation of Meteorological Disasters, Nanjing University of Information Science and Technology, Nanjing 210044, China

[7] CAS Key Laboratory of Marine Geology and Environment, Institute of Oceanology, Chinese Academy of Sciences, Qingdao 266071, China

[8] University of Chinese Academy of Sciences, Beijing 100049, China

Received 9 May 2020; accepted 22 June 2020

© Chinese Society for Oceanography and Springer-Verlag GmbH Germany, part of Springer Nature 2021

Abstract

To assess the performances of state-of-the-art global climate models on simulating the Arctic clouds and surface radiation balance, the 2001–2014 Arctic Basin surface radiation budget, clouds, and the cloud radiative effects (CREs) in 22 coupled model intercomparison project 6 (CMIP6) models are evaluated against satellite observations. For the results from CMIP6 multi-model mean, cloud fraction (CF) peaks in autumn and is lowest in winter and spring, consistent with that from three satellite observation products (CloudSat-CALIPSO, CERES-MODIS, and APP-x). Simulated CF also shows consistent spatial patterns with those in observations. However, almost all models overestimate the CF amount throughout the year when compared to CERES-MODIS and APP-x. On average, clouds warm the surface of the Arctic Basin mainly via the longwave (LW) radiation cloud warming effect in winter. Simulated surface energy loss of LW is less than that in CERES-EBAF observation, while the net surface shortwave (SW) flux is underestimated. The biases may result from the stronger cloud LW warming effect and SW cooling effect from the overestimated CF by the models. These two biases compensate each other, yielding similar net surface radiation flux between model output (3.0 W/m^2) and CERES-EBAF observation (6.1 W/m^2). During 2001–2014, significant increasing trend of spring CF is found in the multi-model mean, consistent with previous studies based on surface and satellite observations. Although most of the 22 CMIP6 models show common seasonal cycles of CF and liquid water path/ice water path (LWP/IWP), large inter-model spreads exist in the amounts of CF and LWP/IWP throughout the year, indicating the influences of different cloud parameterization schemes used in different models. Cloud Feedback Model Intercomparison Project (CFMIP) observation simulator package (COSP) is a great tool to accurately assess the performance of climate models on simulating clouds. More intuitive and credible evaluation results can be obtained based on the COSP model output. In the future, with the release of more COSP output of CMIP6 models, it is expected that those inter-model spreads and the model-observation biases can be substantially reduced. Longer term active satellite observations are also necessary to evaluate models' cloud simulations and to further explore the role of clouds in the rapid Arctic climate changes.

Key words: Arctic Basin, surface radiation budget, cloud radiative effect (CRE), CMIP6 models, CERES, CloudSat-CALIPSO, APP-x

Citation: Wei Jianfen, Wang Zhaomin, Gu Mingyi, Luo Jing-Jia, Wang Yunhe. 2021. An evaluation of the Arctic clouds and surface radiative fluxes in CMIP6 models. Acta Oceanologica Sinica, 40(1): 85–102, doi: 10.1007/s13131-021-1705-6

1 Introduction

Over the Arctic, surface radiation budget, including the incoming solar radiation, reflected shortwave (SW) radiation, and downwelling/outgoing longwave (LW) radiation, is of great importance for the changes of surface temperature and the Arctic sea-ice melt onset and retreat. Arctic surface radiation budget has been widely evaluated in previous studies using observations (Dong et al., 2010; Kay and L'Ecuyer, 2013; Riihelä et al.,

Foundation item: The Major State Basic Research Development Program of China under contract No. 2016YFA0601804; the Global Change Research Program of China under contract No. 2015CB953900; the National Natural Science Foundation of China under contract Nos 41941007 and 41876220; the China Postdoctoral Science Foundation under contract No. 2020M681661.
*Corresponding author, E-mail: zhaomin.wang@hhu.edu.cn; jjluo@nuist.edu.cn

2017), reanalysis products (Perovich et al., 2007; Huang et al., 2017a), and output from climate models (English et al., 2015; Boeke and Taylor, 2016; Lenaerts et al., 2017; Taylor et al., 2019). Many scientific projects or research campaigns have been designed and implemented in the Arctic to understand the underlying processes influencing the Arctic surface energy budget, such as the Surface Heat Budget of the Arctic Ocean (SHEBA, October 1997–October 1998) (Perovich et al., 1999; Uttal et al., 2002; Shupe et al., 2006), the Atmospheric Radiation Measurement (ARM, started in 1989) (Stokes and Schwartz, 1994; Verlinde et al., 2016) and the Arctic Summer Cloud Ocean Study (ASCOS, August–September 2008) (Shupe et al., 2013; Tjernström et al., 2014). The physical processes that determine surface radiation budget in the Arctic involve complicated thermodynamic processes. Up to now, these processes are still poorly understood, especially with the dramatic Arctic climate changes including the rapid sea ice retreat (Kapsch et al., 2013; Huang et al., 2017a; Lee et al., 2017; Huang et al., 2019; Yu et al., 2019) and surface accelerated warming (Serreze and Barry, 2011; Cohen et al., 2014; Walsh, 2014) in recent decades.

Changes in the amount, temperature and optical characteristics (liquid/ice water content, number of droplets and their size) of clouds can modify the surface radiative balance in different ways, known as the surface cloud radiative effect (CRE) or cloud radiative forcing. The cloud water path (CWP), including ice water path (IWP) and liquid water path (LWP), indicates the amount of condensed water (liquid or ice) in a cloud column from cloud base to cloud top of a unit area. In the Arctic, clouds are mainly low-level mixed-phase cloud (Cesana et al., 2012; Van Tricht et al., 2016; Wendisch et al., 2019). CWP is a fundamental physical property of clouds and an important influencing factor determining the radiative effect with different cloud phases. The uncertainty in CWP contributes significantly to the overall uncertainty in cloud-climate feedbacks (Fu and Liou, 1993; Cesana and Storelvmo, 2017). Also, clouds in different height levels and different latitudes have different radiative effects due to discrepancies in temperature and optical depth. Clouds could impact surface radiation budget through two competing processes: reflecting solar SW radiation to space (cooling effect) and trapping the outgoing LW radiation (greenhouse effect) (IPCC, 2014; Li et al., 2011; Matus and L'Ecuyer, 2017). In general, the LW CRE is primarily determined by cloud temperature, height, and emissivity, while SW CRE is determined by the solar zenith angle, surface albedo, and cloud transmittance and albedo. Goosse et al. (2018) summarized several important feedbacks in the polar regions that could influence surface radiative fluxes in a rapidly changing Arctic. Several of those feedbacks are related to changes in the polar cloud cover, such as the positive cloud-sea ice feedback in non-summer months and negative cloud optical depth feedback. The positive feedback depicts that the decrease of Arctic sea ice extent in non-summer months could result in a more low-cloud cover that emits more LW to surface and increases downwelling LW, leading to further sea ice loss. For the latter feedback, the liquid clouds may increase with the Arctic climate warming, which could result in higher cloud albedo and more reflection of SW, dampening the warming process.

Many studies have discussed the surface CREs and their influences on surface temperature or sea ice cover in the Arctic (Liu et al., 2008; Mace and Benson, 2008; Liu and Key, 2014; Letterly et al., 2016; Jun et al., 2016; Huang et al., 2017a, 2019) and Antarctic (Wang et al., 2019). For instance, research in Jun et al. (2016) shows that a large reduction of winter sea ice cover decreased lower tropospheric static stability, leading to enhanced cloud formation and considerable LW radiative forcing based on observations and atmospheric general circulation model (AGCM) experiments. Considering the scarcity and the large uncertainties in the available data sets of Arctic clouds, the variability and changes of Arctic cloud characteristic properties are known little. Until now, no consensus exists on the long-term trend of Arctic total cloud fraction (CF) in the past decades due to the differences of observation methods or available observation periods among different datasets. Possible future trends of Arctic CF projected by different models also show large inter-model spread (Liu et al., 2008; Eastman and Warren, 2010; Liu et al., 2012; Comiso and Hall, 2014; Letterly et al., 2016).

Due to some limitations of the cloud retrieval (availability of daylight and the problems with water path retrieval over ice and snow), available observations of cloud optical parameters in the polar regions are very rare. For instance, most *in situ* observations of Arctic surface radiation and cloud cover during some scientific programs were implemented on a short-term scale and in specific ground sites, such as SHEBA and ASCOS, which are rather limited both temporally and spatially. CWP in moderate resolution imaging spectroradiometer (MODIS) (Platnick et al., 2003) cloud observations only covers the central Arctic during several warm months (April to August) too, as well as another data set CLARA-A2, which stands for "CM SAF cLouds, Albedo RAdiation data record, AVHRR-based, Edition 2" (Karlsson et al., 2017). Thus only a few studies documented the radiative properties of clouds according to their phase in the Arctic. Climate models are great tools for related research. The simulation of cloud physical and optical properties is very important for determining the reliability of climate modeling and climate prediction. Based on available simulation results from coupled model intercomparison project, phase 6 (CMIP6, Eyring et al., 2016) models and several satellite observations, this study intends to evaluate the surface radiation budget and analyze the influence of model-generated cloud properties on surface radiative fluxes over the Arctic.

2 Models, observations and methods

The CMIP6 model outputs of cloud properties and surface radiative fluxes from the atmospheric model intercomparison project (AMIP) experiments (up to December 2014) were analyzed in this study. AMIP experiments were forced by the observed sea surface temperature and sea ice boundary conditions and the model output of these experiments is proper for the comparison with observation products. Only outputs from the first ensemble of each model were analyzed. To date, 22 CMIP6 models provide all variables needed for this study, including CF, cloud LWP, IWP, and surface short-wave/long-wave fluxes in all-sky and clear-sky conditions. The relevant information, including the name, the institution, the atmospheric component and spatial resolution, the cloud fraction scheme, and the references of each model are given in Table 1. According to the work of Qu et al. (2014) and Wang et al. (2015), cloud schemes used in all the 22 models are divided into two diagnostic and one prognostic schemes depending on whether cloud cover is a diagnostic or a prognostic variable. Two types of diagnostic schemes, relative humidity (RH)-based empirical and probability distribution function (PDF)-based statistical schemes, are defined based on the treatment of the stratiform clouds. For RH-based scheme, fractional cloud cover CF is an empirical function of RH. Some RH-based scheme uses the large-scale average condensate (cloud water/ice) as the primary predictor in addition to the grid-mean RH, based on the research of Xu and Randall (1996). In

Table 1. List of the CMIP6 models used in this study with their relevant information

Model	Institution	Atmospheric model	Atmospheric resolution (lon×lat, in degrees or number of grid points)	CF Scheme	References
BCC-CSM2-MR	Beijing Climate Center (BCC)	BCC-AGCM3-MR	320×160 (T106)	RH-based	Wu et al. (2019)
BCC-ESM1	Beijing Climate Center (BCC)	BCC-AGCM3-Chem	128×64 (T42)	RH-based	Wu et al. (2019)
CanESM5	Canadian Centre for Climate Modelling and Analysis, Environment and Climate Change Canada	CanAM5	128×64 (T63)	PDF-based	Von Salzen et al. (2013)
CESM2	National Center for Atmospheric Research (NCAR)	CAM6	288×192	PDF-based	Bogenschutz et al. (2018)
CESM2-FV2	NCAR	CAM6	144×96	PDF-based	Bogenschutz et al. (2018)
CESM2-WACCM	NCAR	CAM6	288×192	PDF-based	Bogenschutz et al. (2018)
CESM2-WACCM-FV2	NCAR	CAM6	144×96	PDF-based	Bogenschutz et al. (2018)
E3SM-1-0	LLNL (Lawrence Livermore National Laboratory), ANL (Argonne National Laboratory), BNL (Brookhaven National Laboratory); LANL (Los Alamos National Laboratory), LBNL (Lawrence Berkeley National Laboratory), ORNL (Oak Ridge National Laboratory), PNNL (Pacific Northwest National Laboratory), SNL (Sandia National Laboratories)	EAM	360×180	PDF-based	Rasch et al. (2019); Zhang et al. (2019)
EC-Earth3	AEMET, BSC, CNR-ISAC, DMI, ENEA, FMI, Geomar, ICHEC, ICTP, IDL, IMAU, IPMA, KIT, KNMI, Lund University, Met Eireann, NLeSC, NTNU, Oxford University; surfSARA; SMHI, Stockholm University, Unite ASTR, University College Dublin, University of Bergen, University of Copenhagen, University of Helsinki, University of Santiago de Compostela, Uppsala University, Utrecht University, Vrije Universiteit Amsterdam, Wageningen University	IFS cy36r4	512×256 (TL255)	Prognostic	Forbes and Ahlgrimm (2012)
EC-Earth3-Veg	same as EC-Earth3	IFS cy36r4	512×256 (TL255)	Prognostic	Forbes and Ahlgrimm (2012)
FGOALS-f3-L	Chinese Academy of Sciences	FAMIL2.2	288×180	RH-based	Xu and Randall (1996); He et al. (2019)
FGOALS-g3	Chinese Academy of Sciences	GAMIL2	180×80	RH-based	Guo and Zhou (2014)
GISS-E2-1-G	NASA Goddard Institute for Space Studies (NASA-GISS)	GISS-E2.1	2.5°×2°	RH-based	Kelley et al. (2020)
INM-CM4-8	Institute for Numerical Mathematics, Russian Academy of Science	INM-AM4-8	2°×1.5°	Prognostic	Tiedtke (1993)
INM-CM5-0	Institute for Numerical Mathematics, Russian Academy of Science	INM-AM5-0	2°×1.5°	Prognostic	Tiedtke (1993)
IPSL-CM6A-LR	Institut Pierre Simon Laplace	LMDZ (NPv6)	144×143	PDF-based	Hourdin et al. (2020)
KACE-1-0-G	National Institute of Meteorological Sciences/Korea Meteorological Administration, Climate Research Division	MetUM-HadGEM3-GA7.1	192×144 (N96)	Prognostic	Walters et al. (2019); Wilson et al. (2008)
MIROC6	The University of Tokyo, National Institute for Environmental Studies, and the Japan Agency for Marine-Earth Science and Technology	CCSR AGCM	256×128 (T85)	PDF-based	Ogura et al. (2017); Tatebe et al. (2019)
MPI-ESM1-2-HR	Max-Planck-Institut fr Meteorologie (Max Planck Institute for Meteorology)	ECHAM6.3	384×192 (T127)	RH-based	Stevens et al. (2013)
MRI-ESM2-0	Meteorological Research Institute	MRI-AGCM3.5	320×160 (TL159)	RH-based	Kawai et al. (2019)
NESM3	Earth System Modeling Center, Nanjing University of Information Science and Technology	ECHAM6.3	192×96 (T63)	RH-based	Cao et al. (2018)
SAM0-UNICON	Seoul National University	CAM5.3 with UNICON	288×192	RH-based	Park et al. (2017); Park et al. (2019)

PDF-based statistical scheme, cloud cover is determined by accounting for the sub-grid scale variability in both total water content and temperature. This variability often assumes some simple probability density functions (PDFs).

We use surface monthly radiative fluxes from the Clouds and Earth's Radiant Energy System Energy Balanced and Filled (CERES-EBAF) version 4.0 (CERES EBAF-Surface_Ed4.0, Kato et al., 2018) onboard the Terra and Aqua NASA satellites. These data can be obtained from the NASA Langley Research Center CERES ordering tool at (http://ceres.larc.nasa.gov/). This product provides global gridded (with 1°×1° spatial resolution), monthly mean clear-sky fluxes, all-sky fluxes, and CREs at the surface from March 2000 to March 2018. It is the first long-term measurements for estimating the Earth's radiation budget (Wielicki et al., 1998). Cloud cover properties in CERES-EBAF (CERES EBAF-TOA_Ed4.0, Loeb et al., 2018) are derived from simultaneous measurements by MODIS Terra between March 2000 to June 2002 and MODIS Terra+Aqua from July 2002 onwards. CERES-EBAF provides a great observational constraint on Arctic Ocean radiative fluxes, but one should keep in mind that the data quality in high latitudes is lower than at lower latitudes because of the viewing geometry, the lower sun elevation angles and clouds being more difficult to discriminate against a cold and/or bright background such as sea ice. In addition, compared to the observed top of atmosphere (TOA) radiative fluxes, surface radiative fluxes in CERES-EBAF are calculated based on the CERES-EBAF TOA observations along with other satellite observations. Previous studies have indicated that this surface radiation product performs better than other products (Zhang et al., 2015; Slater, 2016) due to the TOA observation constraint. However, the validation of these surface radiative fluxes can only be done at specific surface sites with available radiative measurements, which are rare in the Arctic and may thus lead to uncertainties in evaluating the Arctic surface radiation budget. It has been found that the estimated root-mean-square errors (RMSEs) of CERES-EBAF surface downward SW and LW irradiance in the Arctic are 14 W/m^2 and 12 W/m^2 compared to surface observations, while they are 16 W/m^2 and 12 W/m^2 for upward SW and LW (see Table 8 in Kato et al., 2018).

The CERES-MODIS Edition 4A CF observations (Wielicki et al., 1996) are used for the model assessment of the Arctic cloud properties in this study. Different daytime and nighttime retrieval methods for snow or ice-covered surfaces, along with ancillary data and empirical parameterizations are used to derive cloud properties for both pixel and CERES footprint levels (Minnis et al., 2011). Detailed algorithms for CERES-MODIS cloud properties can be referred to previous studies (Minnis et al., 2011; Huang et al., 2017b; Trepte et al., 2019). CFs in CERES-MODIS have been extensively compared with other products and are representative of passive satellite cloud amounts globally (Stubenrauch et al., 2013). The uncertainty of CF in this product is about 7% globally (Minnis et al., 2011). The cloud mask used in this product could identify cloudy or clear areas 90%–91% and 80%–81% of the time during polar day and night (Trepte et al., 2019). When compared to the results based on cloud mask from the ARM/North Slope of Alaska (NSA) surface lidar observations in Barrow, it is found that CERES-MODIS values of CF agrees well with lidar observed CF in late summer and autumn. It only underestimates the lidar observations by less than 10%. However, in spring months, CERES-MODIS values fall short of their lidar counterparts by 20%–30%. The RMSE between them peaks in March to April (~40%) and bottoms out to about 10% in August (Spangenberg et al., 2004). CWPs obtained from CERES-MODIS show large uncertainties compared to other observation products especially in high latitudes. For example, over the Arctic, the mean differences and correlation coefficients of the retrieved LWPs relative to the ARM/NSA ground-based observations are 5.6 g/m^2 and 0.59 over snow conditions (Dong et al., 2016). Thus they are not used in this study.

To better investigate cloud conditions over the Arctic region, we also utilized CF data from Extended AVHRR Polar Pathfinder (APP-x) (Wang and Key, 2005a, 2005b; Key et al., 2014, 2016). The retrieval of APP-x cloud properties is specifically designed for polar AVHRR daytime and nighttime data. CF is retrieved at high and low sun times using a radiative transfer model FluxNet and a suite of algorithms (Wang and Key, 2005a). APP-x data products are mapped to a 25 km EASE-grid. Daily APP-x cloud observations are available from the year 1982 until present and can be obtained from the National Centers for Environmental Information (NCEI) of National Oceanic and Atmospheric Administration NOAA (https://www.ncdc.noaa.gov/cdr/atmospheric/extended-avhrr-polar-pathfinder-app-x). It is a thematic climate data record to provide information on surface and cloud properties and radiative fluxes. The uncertainty of APP-x CF over the study area of SHEBA is about 26% (Key et al., 2016). The comprehensive set of variables in APP-x can be used to study trends and interactions within the Arctic climate systems, yet the cloud water path data is not available.

Another data set, which is known as the collocated radar CloudSat and lidar CALIPSO, hereafter abbreviated as CloudSat-CALIPSO, is of even superior quality to the CERES-MODIS and APP-x cloud property data sets. This data set merges the CloudSat geometrical profiling product (GEOPROF) (with a vertical resolution of 240 m) (Marchand et al., 2008) and the CALIPSO Vertical Feature Mask (VFM) (with a vertical resolution of 60 m) (Vaughan et al., 2009). The CALIPSO VFM data is valuable for assessing changes in low (<720 m) and geometrically thin cloud cover (Kay and Gettelman, 2009; Mace et al., 2009). A combination of the data obtained with both sensors allows obtaining an almost complete characterization of the vertical cloud structure because the two sensors couple with their different wavelengths used to the different cloud and precipitation particles of both phases, liquid and solid. The uncertainty of global CF in CloudSat-CALIPSO monthly mean product is about 5% (Mace et al., 2009). As pointed out by Kay and L'Ecuyer (2013), CloudSat-CALIPSO is highly valuable to cloud study due to the active cloud detection technique and the ability to provide vertical cloud distributions. However, the collocated data set is only available for a much shorter period (from June 2006 to February 2011) and has an observational "pole hole" from 82°N to 90°N. Thus the gridded monthly CloudSat-CALIPSO cloud cover data offered by the Integrated Climate Data Centre (ICDC), CEN, University of Hamburg (https://icdc.cen.uni-hamburg.de) was only used to verify the CF observations from CERES-EBAF and APP-x in this study.

Previous studies have pointed out that the large model-observation bias and the inter-model spread of the CF amount are partly due to the lack of a common algorithm and spatial scale used when calculating cloud properties in models and in satellite observations (Webb et al., 2017). Yu et al. (1996) firstly introduced the "satellite simulator" method based on satellite observations from the International Satellite Cloud Climatology Project (ISCCP), which uses the same data processing system as the satellite to handle and output the model data. Thus a satellite simulator integrated in a certain model can be used to diagnose the directly observed cloud and radiation parameters by the satellite sensor, making the model assessment against satellite

observations more accurate and credible (Bodas-Salcedo et al., 2011). In the first phase of the Cloud Feedbacks Model Intercomparison Project (CFMIP-1) implemented by the World Climate Research Programme (WCRP) (McAvaney and Le Treut, 2003), only two groups of experiments (AMIP and 2xCO2) including ISCCP simulator were executed. Since CFMIP-2, the CFMIP Observation Simulator Package (COSP) (Bodas-Salcedo et al., 2011), including the ISCCP simulator, CALIPSO simulator, MODIS simulator, et al., was provided for different model development centers. Satellite simulators in COSP have also been integrated into CMIP6 models for implementing the CFMIP-3 model experiments.

The reference area analyzed in this study is the Arctic Basin. The domain of the Arctic Basin is defined the same as that in Wei et al. (2019) (in their Fig. 1), which covers the ocean area north of 70°N, excluding the Nordic Seas, the Barents sea, and the Baffin Bay (Fig. 1). Basin-averaged values are calculated on the original grid of each CMIP6 model and each observation dataset, while for the spatial maps of multi-model mean and inter-model spread, as well as the spatial distribution of model-observation differences, all data sets are re-gridded onto a 2° (longitude) × 1° (latitude) grid. Note that in this study the four seasons are defined as follows: winter (December–February), spring (March–May), summer (June–August) and autumn (September–November).

3 Results

3.1 *Mean Arctic Basin surface radiative fluxes*

Figures 2–7 present the spatial patterns, climatological annual means, and seasonal cycles of Arctic Basin surface radiative fluxes from both CMIP6 models and CERES-EBAF. For the Arctic Basin, both the individual radiation component and the net radiation fluxes show consistent spatial patterns in the multi-model mean and in CERES-EBAF, with obvious latitudinal gradients modified by the occurrence of topography (Figs 2, 4 and 6). Simulated incoming shortwave (SW) radiative flux is lower than observation within the Arctic Basin. Surface upward SW radiative flux is mainly determined by the surface albedo and the amount of downward component, with maximum values in the Greenland due to the high albedo of the Greenland Ice sheet (Fig. 2). Surface SW radiative flux from October to February is nearly zero, while the maximum SW occurs in summer months (June, July, and August) following the seasonal variation of solar elevation angle (Fig. 3). Net annual SW radiative flux within the Arctic Basin is about 5.3 W/m^2 lower than in the CERES-EBAF (Fig. 3). The spread among different models and the model-observation bias may come from different surface or cloud properties.

The spatial distribution and the variation of downward longwave (LW) radiative flux are closely related to the vertical structures of the boundary layer and the cloud fraction and optical properties, while upward LW radiative flux highly depends on the surface temperature. On the contrary to net SW radiative flux, net LW radiative flux is increasing with latitude in the Arctic Ocean (Fig. 4). Compared to CERES-EBAF, downward LW is overestimated by the models, which may be related to the model biases in cloud properties and the cloud radiative forcing. Net LW radiation in the Arctic Basin is negative all year round (Fig. 5). In CMIP6 multi-model mean, net LW radiative flux is greater than

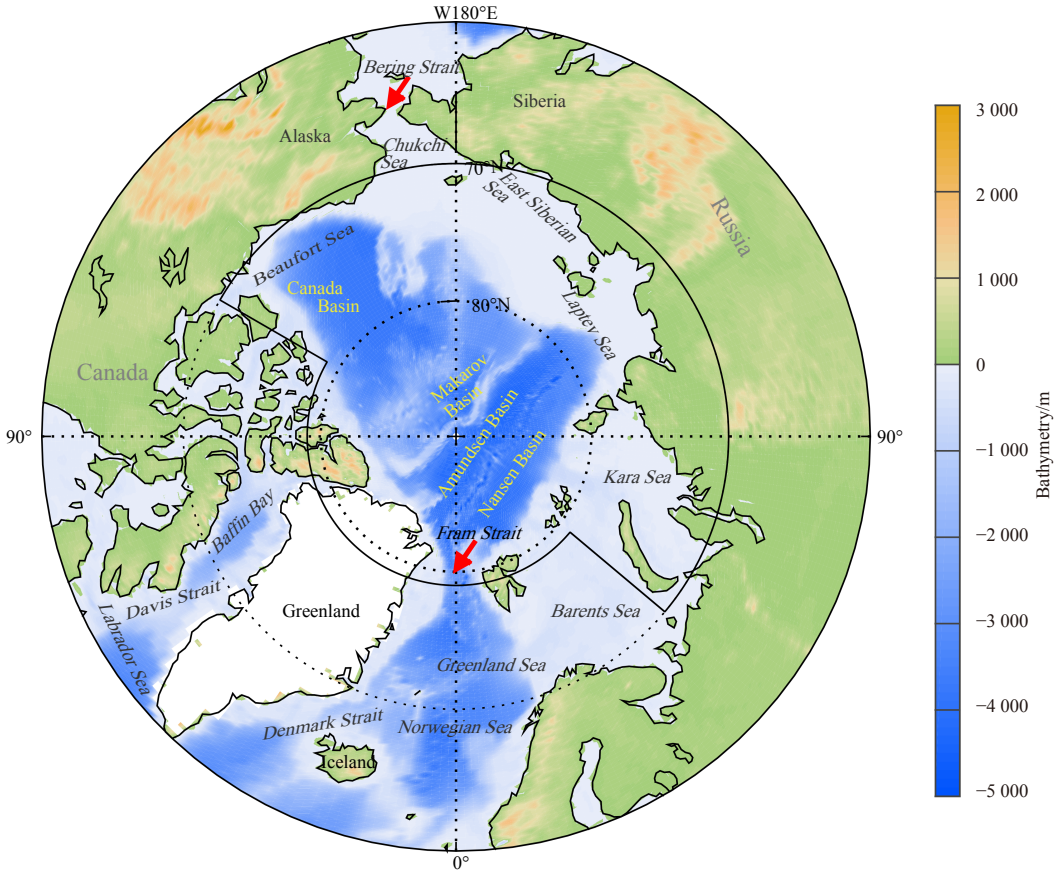


Fig. 1. Bathymetry of the Arctic region derived from ETOPO1. The black curve highlights the domain of the Arctic Basin defined in this study. This figure is a revised version of Fig. 1 of Wei et al. (2019).

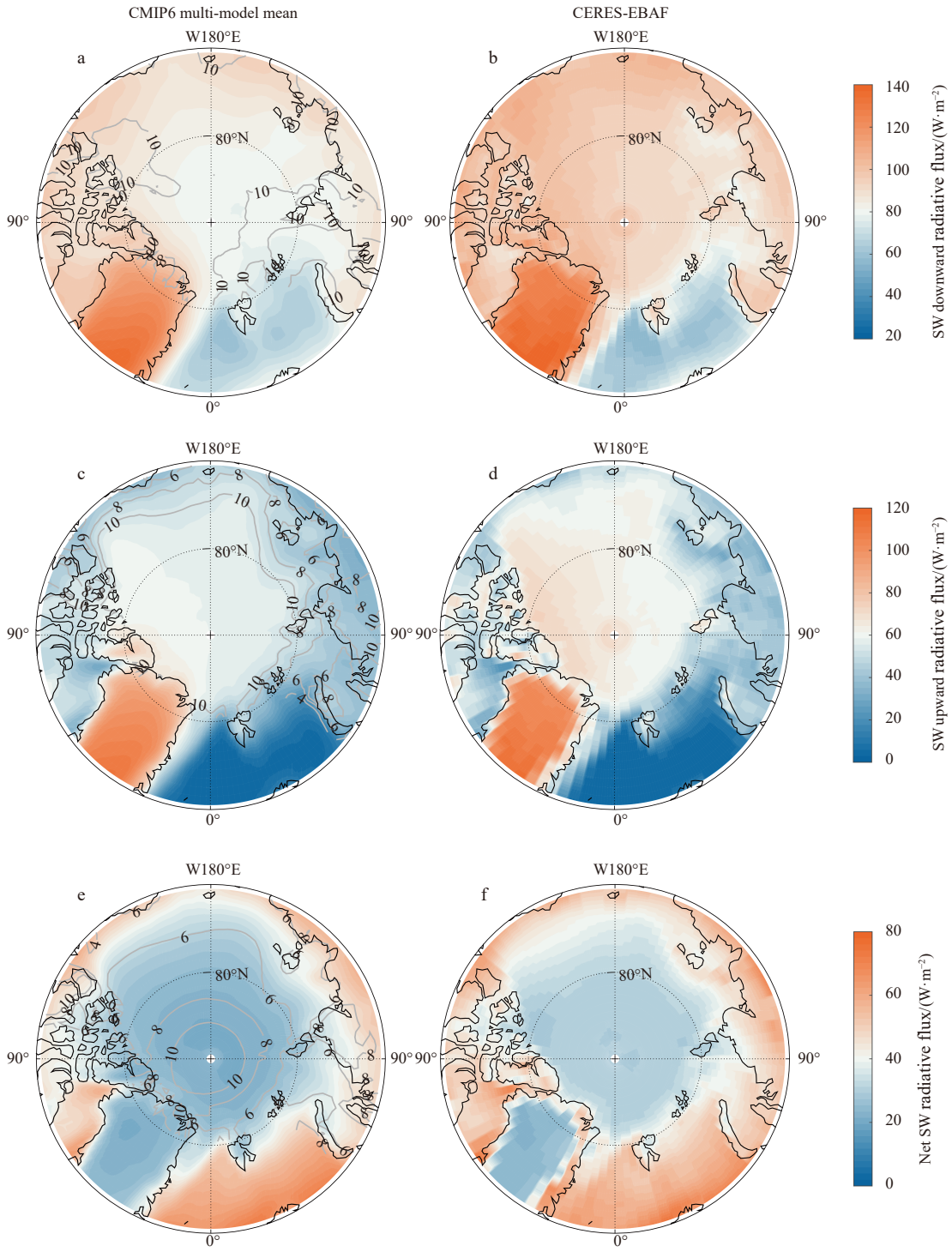


Fig. 2. Climatological maps of annual mean Arctic Basin surface shortwave (SW) radiative fluxes over 2001–2014: CMIP6 multi-model mean (left) and CERES-EBAF (right) surface downward, upward, and net SW radiative fluxes. Contours in the left panels represent the inter-model spreads, i.e., the standard deviation among different models. The upward component is positive up and the downward and net radiation is positive down.

CERES-EBAF for all 12 months (especially in warm months), leading to 8.4 W/m^2 overestimation of annual mean LW radiative flux (Fig. 5e). This overestimation means that the surface energy loss by LW is not enough in the models. Annual mean LW radiative flux from FGOALS-g3 (–37.1 W/m^2) and KACE-1-0-G (–36.5 W/m^2) is mostly close to CERES-EBAF (–36.9 W/m^2). The seasonal variation of net LW radiative flux differs significantly between CMIP6 and CERES-EBAF. Winter net LW radiative flux in CMIP6 is lower than summer, quite different from that in CERES-EBAF (Fig. 5f).

For net surface radiation, underestimation of SW radiative flux and overestimation of LW radiative flux in CMIP6 are partially canceled each other out and result in an overestimation of

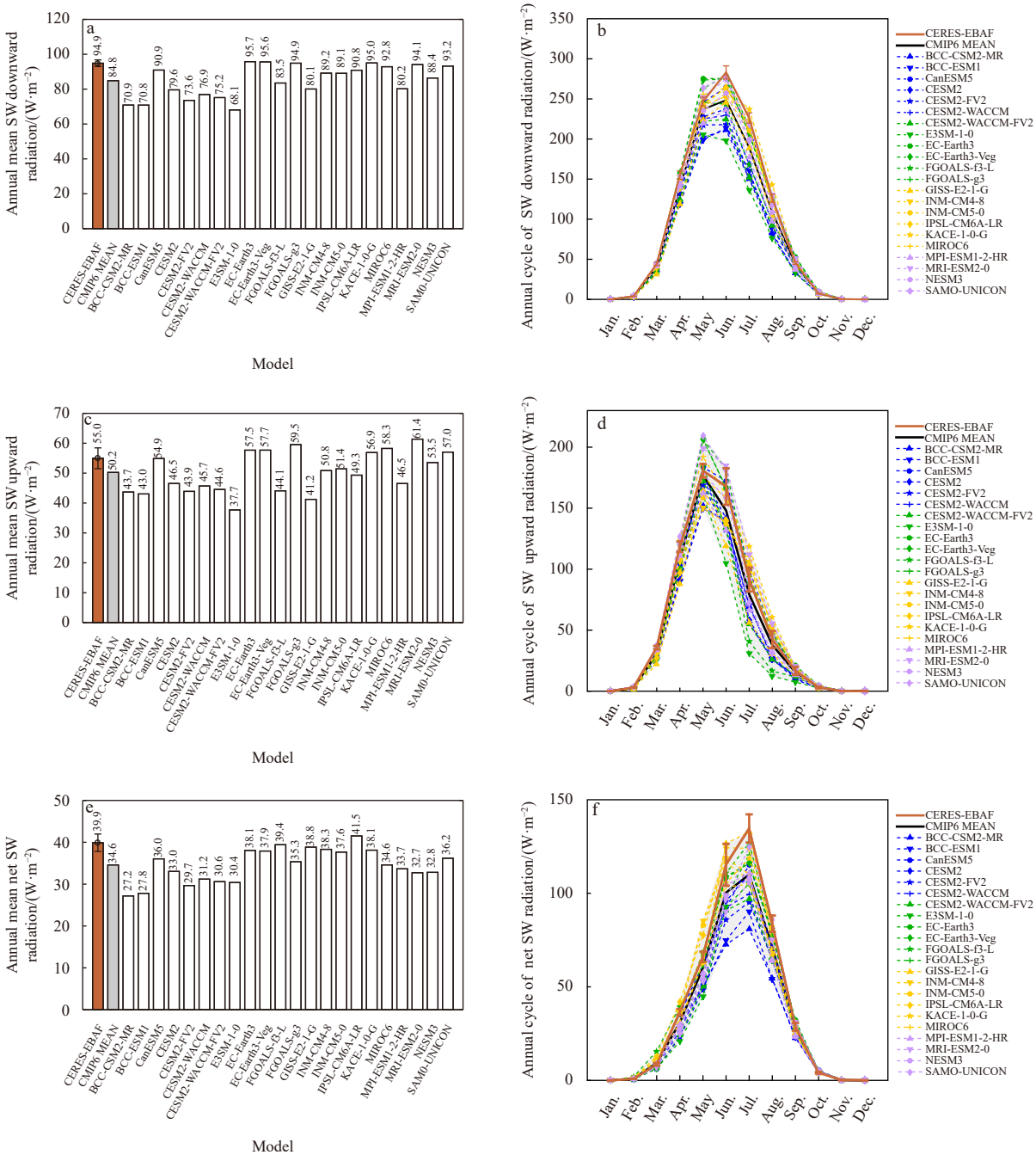


Fig. 3. Arctic Basin annual (left) and monthly (right) surface downward (a, b), upward (c, d), and net (e, f) shortwave (SW) radiation from CERES-EBAF and 22 CMIP6 models over 2001–2014. The gray shaded areas in the right panels indicate the range of the models. The error bars of CERES-EBAF annual mean and monthly radiative fluxes in 14 years are also shown.

3.1 W/m² in annual net surface radiation in the Arctic Basin (Figs 6 and 7). Simulated annual mean net surface radiation fluxes are positive in most models except for EC-Earth3, EC-Earth3-Veg and FGOALS-g3. In the Arctic Basin, the RMSEs of basin-wide annual averaged radiation between CMIP6 multi-model mean and CERES-EBAF are 5.5 W/m², 8.6 W/m² and 3.5 W/m² for net SW, net LW and net radiation, respectively. According to previous studies, large biases in surface radiation budget stem from improper parameterizations of radiative transfer algorithms or cloud schemes in different climate models (Christensen et al., 2016). The spatial pattern of SW, i.e., decreasing with latitude, is consistent between models and CERES-EBAF, while for LW and net radiation, some distinct discrepancies exist. While CMIP6 multi-model mean reveals a uniform distribution of net SW within central Arctic Basin, the unrealistically net LW/net radiation increase north of about 82°N in CERES-EBAF seems to result from the limitation for MODIS cloud detection in very high-latitudes, as mentioned in Section 2.

3.2 *The cloud climatology over the Arctic Basin*

Figure 8 shows the spatial distribution of seasonal mean Arctic CF in CMIP6 model and satellite observations during the

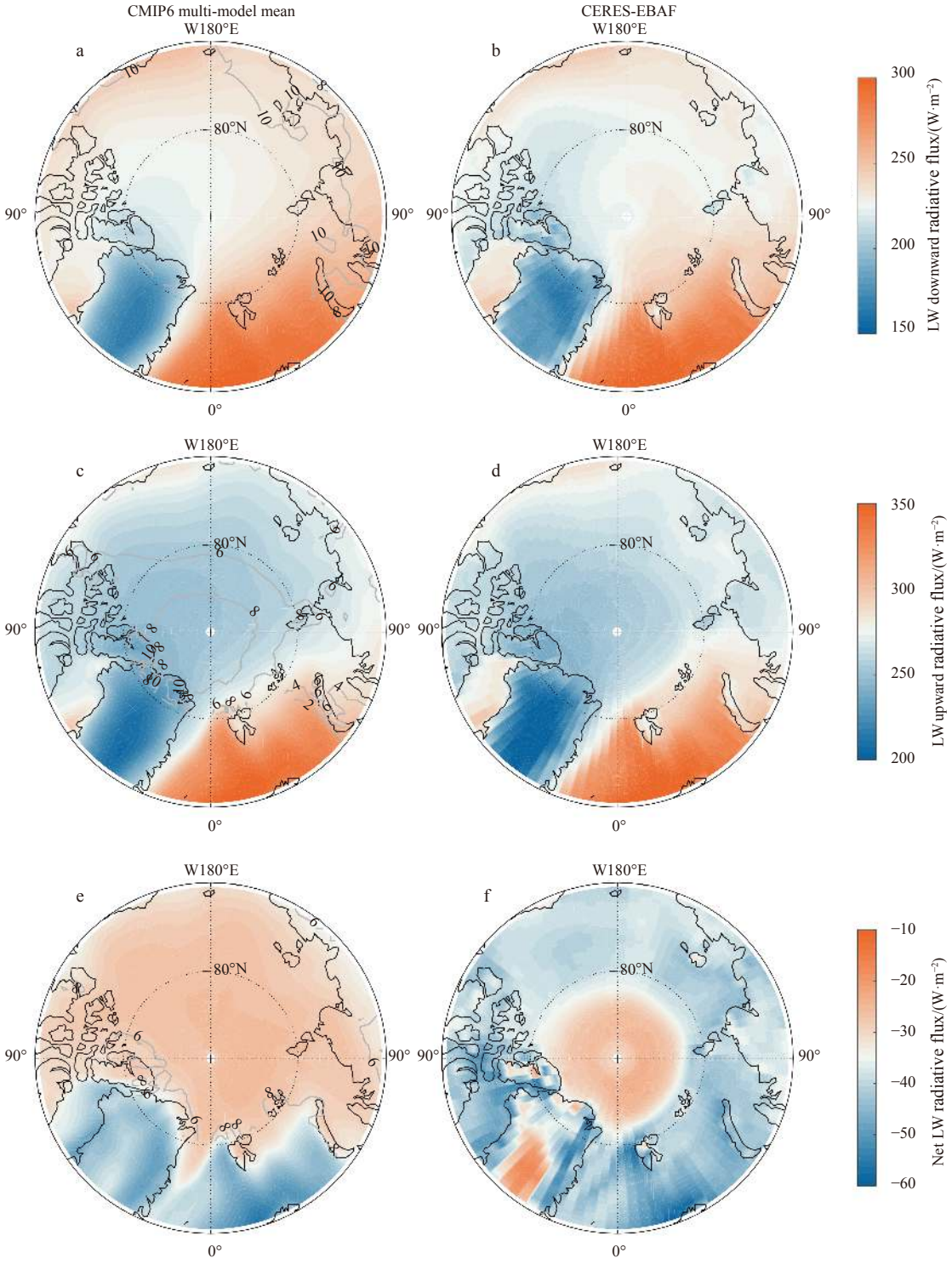


Fig. 4. Climatological maps of annual mean Arctic Basin surface longwave(LW) radiative fluxes over 2001–2014: CMIP6 multi-model mean (left) and CERES-EBAF (right) surface downward, upward, and net LW radiative fluxes. Contours in the left panels represent the inter-model spreads, i.e., the standard deviation among different models. The upward component is positive up and the downward and net radiation is positive down.

available period for CloudSat-CALIPSO (2007–2010). In summer and autumn, CERES-MODIS CF is much higher than the other two observations, while the winter CF in APP-x is higher than that in CloudSat-CALIPSO and CERES-MODIS. The general spatial patterns of CF in 3 observation products are successfully reproduced in CMIP6 models except for summer. High CF is located in the Atlantic sector, which is mainly due to the high atmospheric humidity and temperature over the open water and the frequent storm activity over this area. Low CF in the Pacific sector, the central Arctic Ocean and the Canadian Archipelago is related to the strong anticyclones over those regions and lack of moisture (Liu et al., 2012). However, the simulated CF amounts over the

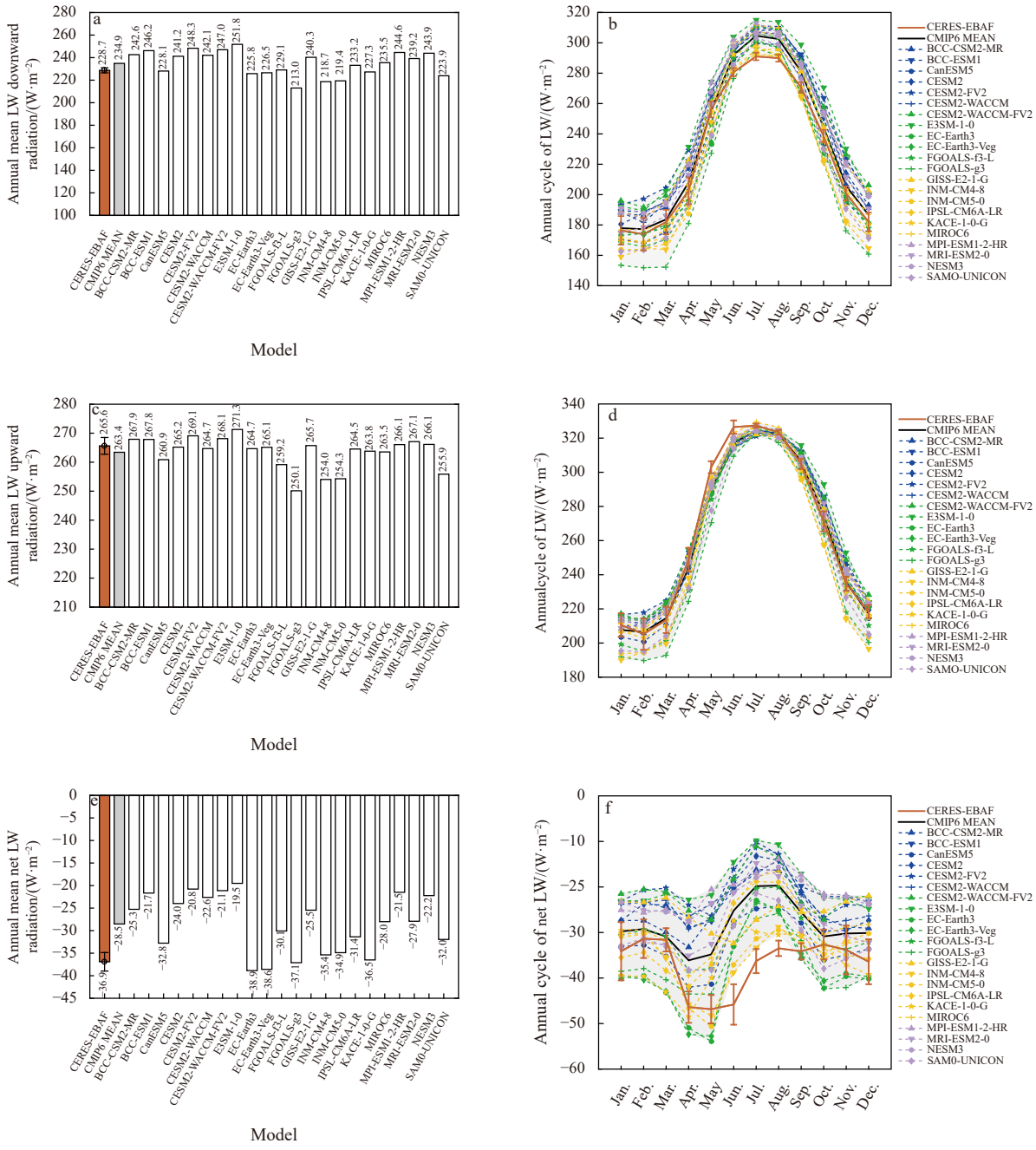


Fig. 5. Arctic Basin annual (left) and monthly (right) surface downward (a, b), upward (c, d), and net (e, f) longwave (LW) radiation from CERES-EBAF and 22 CMIP6 models over 2001–2014. The gray shaded areas in the right panels indicate the range of the models. The error bars of CERES-EBAF annual mean and monthly radiative fluxes in 14 years are also shown.

whole study region are substantially overestimated compared to observations.

To compare the modeled area-weighted average of annual mean and seasonal cloud fractions with results from different remote sensing products (CERES-MODIS, APP-x, and CloudSat-CALIPSO), the analysis of all datasets is constrained in the same region (Arctic Basin) and within the same time period (2007–2010). Table 2 shows that there are some common features among different cloud products. For all data sets, largest CF occurs in autumn, while winter and spring experience the least cloud cover. CFs detected in CloudSat-CALIPSO are lower than in CERES-MODIS and APP-x in all seasons, partly due to the "pole hole" in CloudSat-CALIPSO observations. Winter CF in APP-x is much higher than those in the other two observations, possibly resulting from the poor discrimination of thick clouds and ice-covered surface (with comparable reflectance) in APP-x. The RMSE of 2007–2010 annual mean Arctic Basin CF between CloudSat-CALIPSO and CERES-MODIS (about 7.6%) is slightly lower than that between CloudSat-CALIPSO and APP-x (around 8.0%).

For 2001–2014, the annual CF in CMIP6 multi-model mean is about 84.9%, closer to APP-x and slightly higher than CERES-MODIS (Fig. 9). Obviously, the error bars show that the observed inter-annual variation of the CF is much lower in July–October

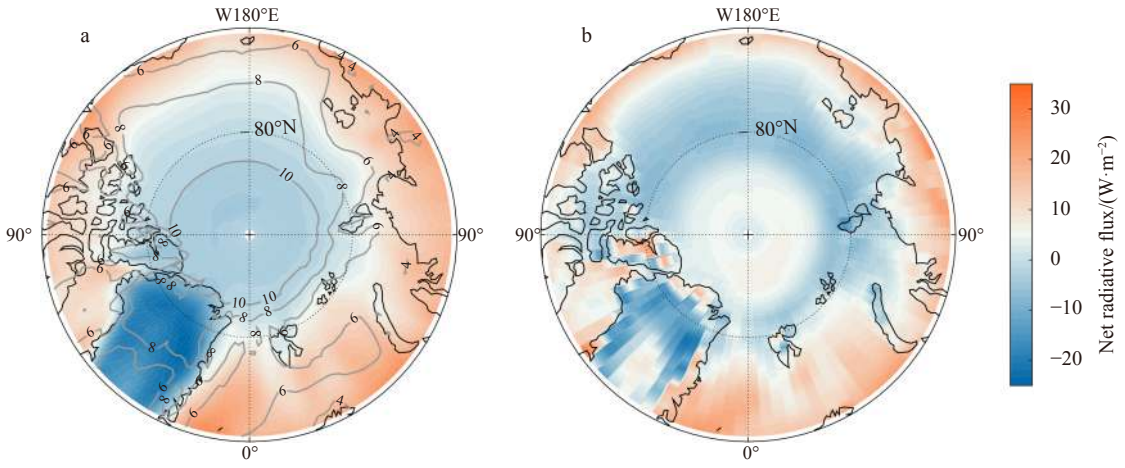


Fig. 6. Climatological maps of annual mean Arctic Basin surface net radiative fluxes over 2001–2014 from CMIP6 multi-model mean (a) and CERES-EBAF (b). Contours in the left panel represent the inter-model spreads, i.e., the standard deviation among different models. The net radiation is positive down.

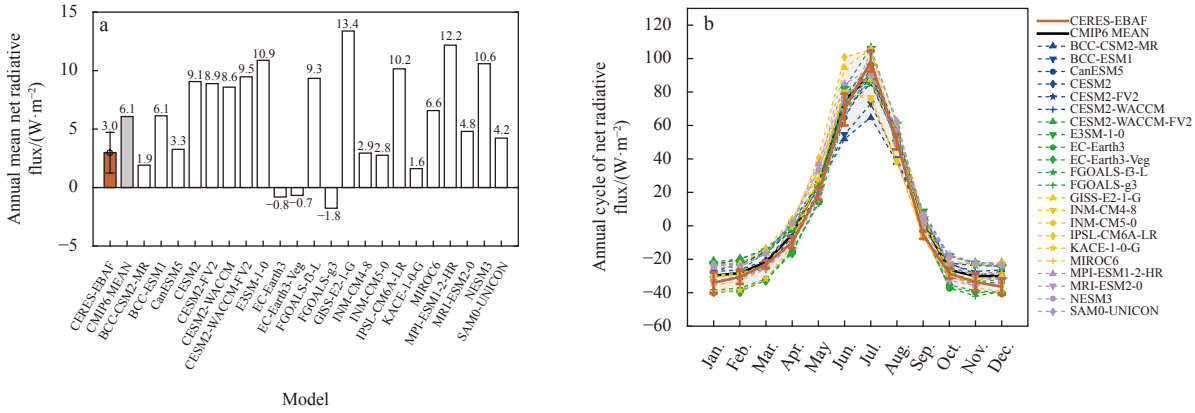


Fig. 7. Arctic Basin annual (a) and monthly (b) surface net radiative fluxes from CERES-EBAF and 22 CMIP6 models over 2001–2014. The gray shaded areas in the right panels indicate the range of the models. The error bars of CERES-EBAF annual mean and monthly radiative fluxes in 14 years are also shown.

than in other months (same as in CMIP6 multi-model mean, but not shown in the figure). Cloud formation are mainly controlled by large-scale atmospheric circulation and local turbulent fluxes between ocean and atmosphere (Kay and Gettelman, 2009). From winter to spring, atmospheric circulation generally shows more significant variations, which may explain the higher variations of CF than in late summer and autumn. More cloud in autumn and less cloud in winter and spring are consistent in two observations and in CMIP6 multi-model mean. A more cloudy state in autumn is related to the surface properties and the air-sea interactions in the Arctic. Near-surface static stability significantly affects cloud formation and evolution. Low clouds form extensively over newly open water in the early autumn. The relatively low static stability in autumn favors the upward turbulent fluxes of heat and moisture, which may result in more CF in autumn than in spring (Kay and Gettelman, 2009). CF in CERES-MODIS shows a more “fluctuating” seasonal changes, while in CMIP6 multi-model mean and APP-x, the seasonal variation is much weaker.

Generally, seasonal variations of CF modeled by different models are consistent with observations. However, the great spread of CF (especially in winter and spring) among the CMIP6 models makes it difficult for the comparison between different data sets. For example, BCC-CSM2-MR, FGOALS-g3, and MIROC6 exhibit strong seasonal cycles similar to CERES-MODIS, but four CESM2 models (CESM2, CESM2-FV2, CESM2-WACCM, and CESM2-WACCM-FV2) have small fluctuations with the CF being larger than observations throughout the year. Seasonal cycles of CF in CMIP6 models are consistent with CMIP5 models, but the spread of CF among CMIP6 models is much smaller than that in CMIP5 (Boeke and Taylor, 2016) if the extremely low CF from FGOALS-g3 is excluded. The negative net radiative flux in FGOALS-g3 (Fig. 7a) is probably related to its underestimation of CF. Note that the methods to calculate CF are totally different between models and satellite retrievals, resulting in the large inter-model spread and the differences between modeled and observed CF (Qu et al., 2014; Huang et al., 2017a). In general, models using PDF-based (e.g., four CESM2 models and E3SM-1-0) and prognostic (e.g., two INM-CM models and two EC-Earth3 models) CF schemes simulate more cloud cover than those using RH-based empirical scheme (e.g., MIROC6 and FGOALS-g3), although most models overestimate the total CF compared to observations. The different horizontal and vertical resolutions are also potentially inducing large inter-model spreads and large dif-

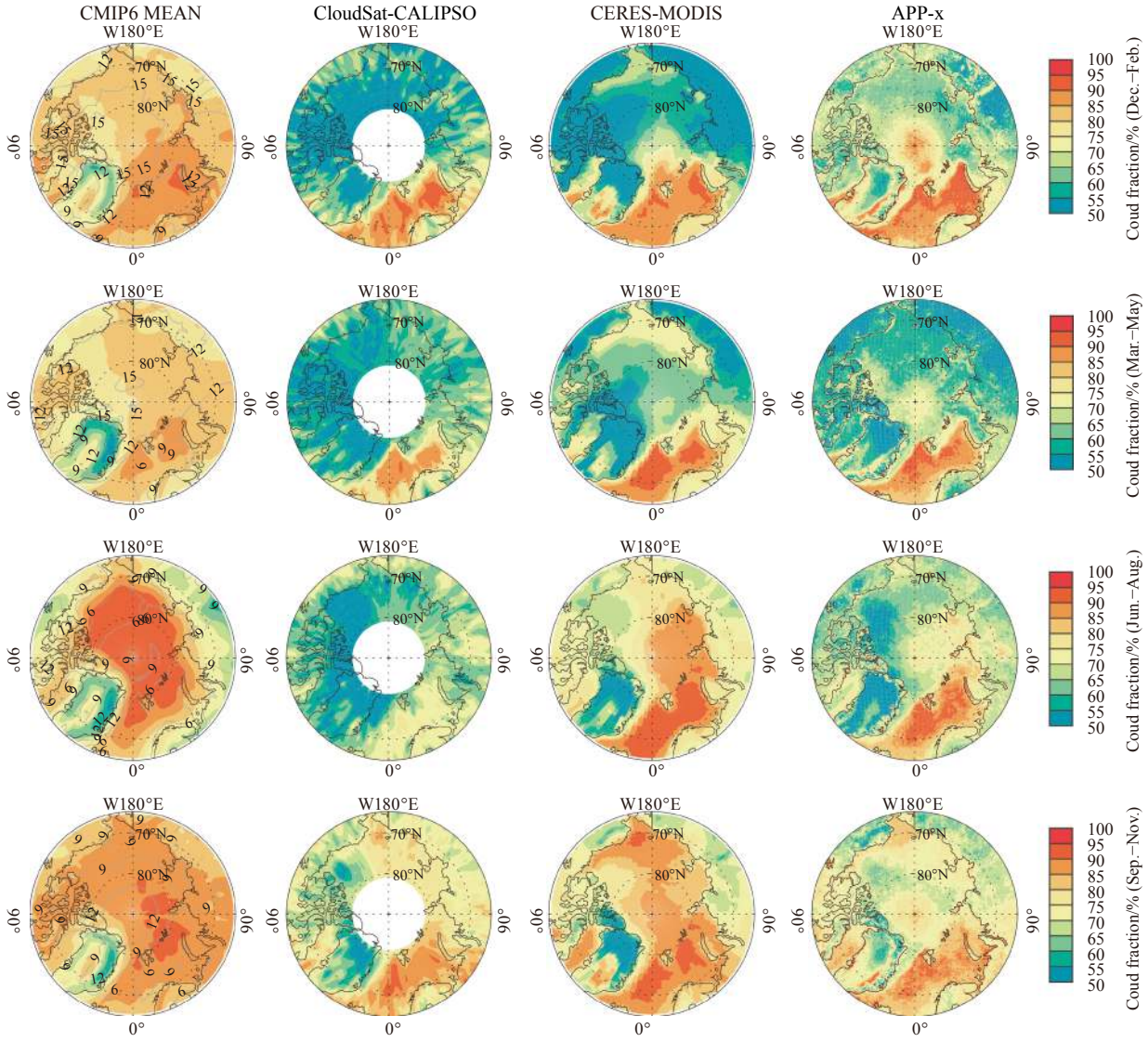


Fig. 8. Climatological maps of seasonal mean Arctic cloud fraction (CF) over January 2007–December 2010 from CMIP6 multi-model mean (the first column) and three observations (CloudSat-CALIPSO, CERES-MODIS and APP-x) (the second to the fourth columns). Contours in the first column represent the inter-model spreads, i.e., the standard deviation among different models

Table 2. Arctic Basin total cloud fraction (CF) in 2007–2010 from different products

	CF/%				
	Winter	Spring	Summer	Autumn	Annual mean
CMIP6 MEAN	84.0	81.3	87.0	87.5	84.9
CloudSat-CALIPSO	59.1	60.6	60.6	74.6	63.9
CERES-MODIS	59.8	65.6	78.9	82.1	71.4
APP-x	72.4	66.3	71.0	77.2	71.7

ferences between modeled and observed CF, especially when doing the regional averaged analysis after resampling the data.

In order to minimize the impacts of inconsistent algorithms and spatial resolutions used to calculate CF in models and observations, COSP outputs of CMIP6 models are also analyzed. At present, COSP outputs of CALIPSO and MODIS from three models (BCC-CSM2-MR, IPSL-CM6A-LR and MRI-ESM2-0) are available. The derived climatological spatial patterns and seasonal cycles of CF are compared with the original model outputs and the corresponding observations (Figs 10 and 11). It is obvious that the use of satellite simulator could significantly reduce the model-observation differences of CF in cold seasons and in the central Arctic Ocean, especially for the model IPSL-CM6A-LR. Moreover, the inter-model spreads of monthly CF are also smaller than those in the original model results in autumn, winter, and spring (Fig. 11). Therefore, reduced model-observation discrepancies can be expected if more COSP outputs of CMIP6 models are released.

Basin-averaged cloud CWP and LWP in Arctic Basin show common seasonal changes in all CMIP6 models, with the highest in July to September and lower in other months (Figs 12a and b). The persistent high LWP in summer and fall is consistent with the

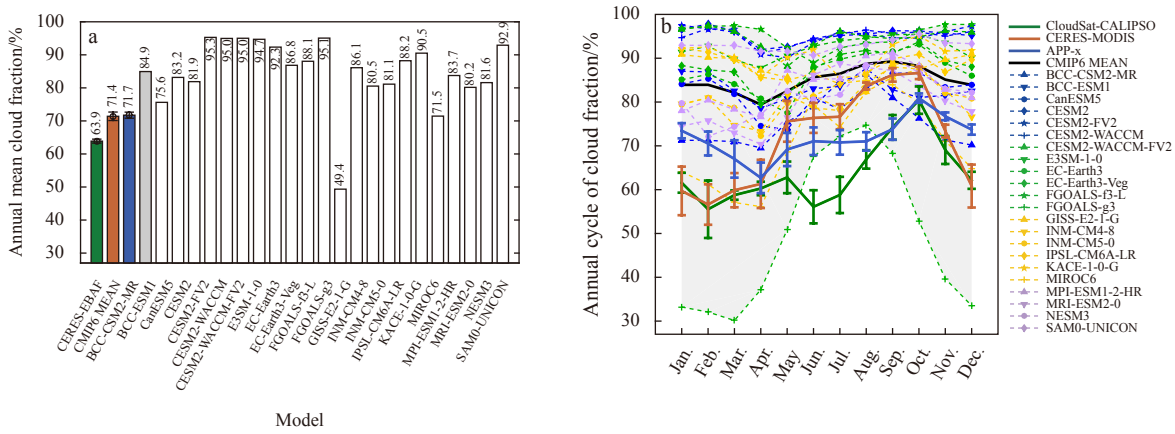


Fig. 9. Arctic Basin annual (a) and monthly (b) CF from 22 CMIP6 models, CERES-MODIS and APP-x averaged over 2001–2014. The gray shaded area in b indicates the range of the models. The error bars of observed annual mean and monthly CF from observation products in 14 years are also shown.

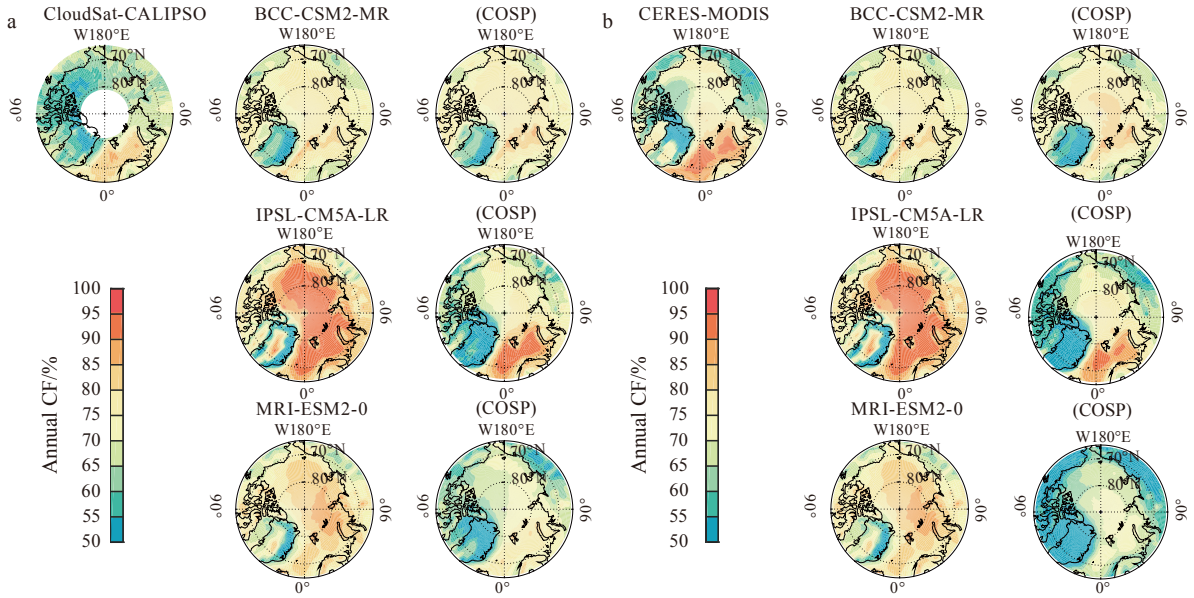


Fig. 10. Climatological maps of annual Arctic CF from CloudSat-CALIPSO (a) and CERES-MODIS (b) as well as CMIP6 models' none-COSP and COSP output during 2007–2010 (a) and 2001–2014 (b).

results based on the GCM-Oriented CALIPSO (CALIPSO-GOCCP) product (Cesana et al., 2012), although a different area of 60°–82°N was focused due to the pole hole in CALIPSO observations. Compared to LWP, the IWP of clouds over the Arctic Ocean is relatively constant over the year, with little seasonal variation (Fig. 12c). This is in consistent with the 4-year CloudSat-CALIPSO observations for the whole Arctic shown in Lenaerts et al. (2017). IWP seasonal cycles present a relatively large inter-model spread. Multi-model mean IWP is the smallest in early summer (May–July) and the greatest in early autumn (September and October). The disagreements in CWPs among different models possibly result from different cloud parameterization schemes used to determine polar cloud properties.

3.3 *Arctic Basin cloud radiative effect (CRE)*

It is shown in Fig. 13 that the seasonal evolution of net surface CRE in the Arctic is mainly dominated by the SW CRE both in CMIP6 and in CERES-EBAF. The cloud SW cooling effect and LW warming effect all year round in CMIP6 are also consistent with previous studies (Kay and L'Ecuyer, 2013; Boeke and Taylor, 2016). Annually, both the cooling effect and the warming effect in CMIP6 mean are slightly overestimated compared to CERES-EBAF. Net CRE in Arctic Basin is only negative from June to August, indicating the significant "cloud SW albedo effect" that surpasses the "cloud LW warming effect" in summer months. Annual mean total net CRE is 20.2 W/m^2 in CMIP6 model mean, about 1.3 W/m^2 slightly higher than CERES-EBAF. In comparison, globally, clouds contribute to a negative surface radiative effect by reflecting more SW than they trap LW radiation (Cesana and Storelvmo, 2017), reflecting the spatial discrepancy of cloud effects on surface radiation. In the next section, the impacts of Arctic Basin CF and CWP onto the CREs in different seasons are preliminarily estimated.

Based on CMIP6 model results, the area-weighted averaged

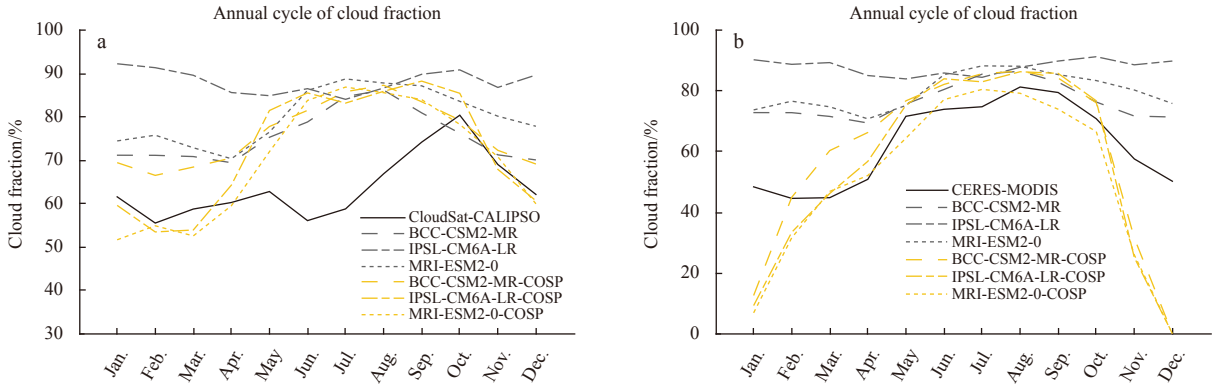


Fig. 11. Arctic Basin monthly CF from CloudSat-CALIPSO (a) and CERES-MODIS (b) and CMIP6 models' none-COSP and COSP output averaged over 2007–2010 (a) and 2001–2014 (b). Note that the CloudSat-CALIPSO has an observational "pole hole" from 82°N to 90°N.

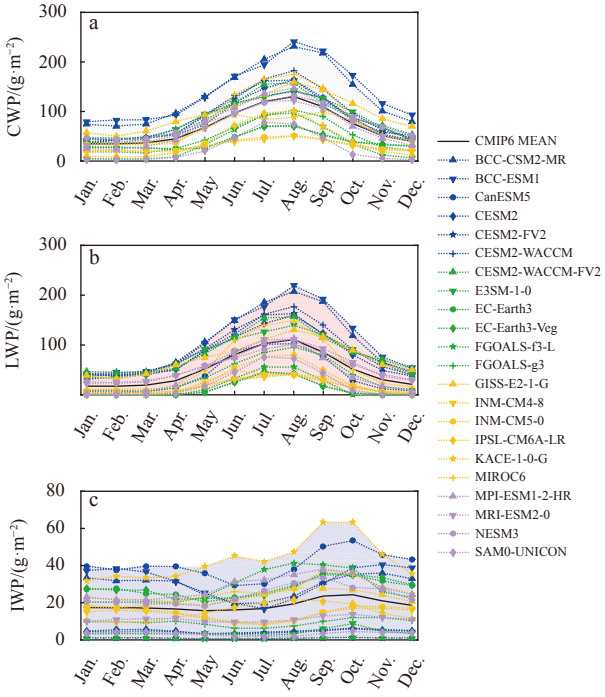


Fig. 12. Monthly Arctic Basin cloud water path (CWP) (a), liquid water path (LWP) (b), and ice water path (IWP) (c) averaged during 2001–2014. The shaded regions indicate the range of the models.

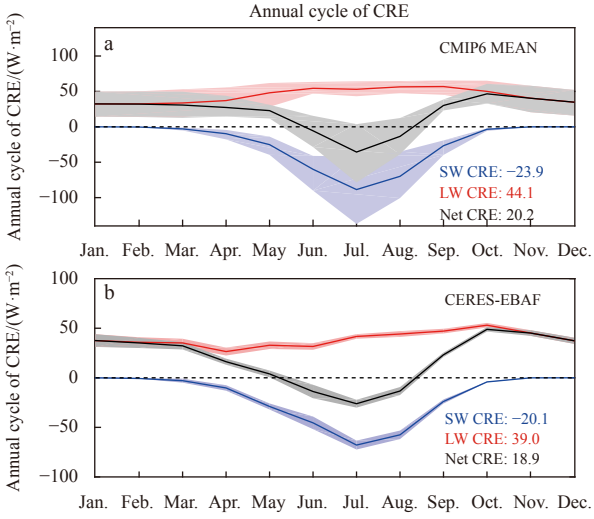


Fig. 13. Monthly Arctic Basin cloud radiative effects (CREs) during 2001–2014: CMIP6 (a) and CERES-EBAF (b) multi-model mean surface SW CRE, LW CRE, and total CRE. Numbers in a and b represent annual mean CREs for SW, LW and net radiation. The shaded areas in a and b indicate the ranges of the models and the standard deviations of CERES-EBAF monthly CREs, respectively.

CF and CWP in the Arctic Basin show sufficiently different impacts onto CREs. The scatterplots in Figs 14 and 15 represent the relationships between Arctic cloud properties and different components of CREs. Each dot stands for the seasonal mean value of CF/CWP (horizontal axis) and CRE (vertical axis) in each year. The linear regression lines for the dots on each scatterplot are given. According to the determination coefficient (R^2) of each fitting line, it is found that the "greenhouse effects" of CF, CWP and LWP on net LW are prominent during winter (Fig. 14), while these effects are significant for CF and CWP in spring (Fig. 15). In the CERES observations, the LW warming effect of CF in winter is also significant (figure is omitted). The SW cooling effect of CF is prominent in spring. The relationships between CREs and CF/CWPs shown in the scatterplots are only based on short-term (14-year) model outputs and CERES observations, and are limited only in part of the Arctic. In the near future, detailed analysis will be conducted on the different CREs from different cloud properties, such as cloud base height, cloud size, cloud types, et al., using more available observations in the Arctic. As pointed by Goosse et al. (2018), the presence of different phases of water in polar regions implies that many processes and feedbacks are highly nonlinear. Results in Figs 14 and 15 may include effects from other climate parameters or other climate feedbacks (such as the positive cloud-sea ice feedback).

3.4 *Variability of and changes in the Arctic Basin surface radiation budget*

Figure 16 shows the annual mean net surface radiation in the Arctic Basin during 2001–2014, as well as the annual CF and CWPs. The year-to-year changes in CMIP6 net surface radiation

is well correlated with those in CERES-EBAF before the year 2008 (with a correlation coefficient of 0.95). Possible causes for the weak correlation after 2008 is unknown at present. Several possible reasons could result in the difference in cloud inter-annual variation between models and observations shown in Fig. 16b, including the poor satellite cloud detection quality in winter and in polar regions (Liu et al., 2010), as well as the deficiencies in the model's cloud parameterization schemes (Qu et al., 2014).

Net surface radiation shows no obvious trend in both CERES-EBAF and CMIP6 model mean (figure omitted). Among all seasons, autumn CF in CERES-MODIS shows significant decreasing trend (–0.38% per year, figure is omitted) that is consistent with in situ observations from ARM/NSA (Dong et al., 2010), but not consistent with other studies such as Huang et al. (2017a). Annual and spring CFs in CMIP6 multi-model mean increase significantly, with the linear trends of 0.07% and 0.16% per year (Fig. 17). Generally, most models show increasing trends of seasonal mean CF (especially spring CF) during 2001–2014, but only a few are significant enough. Different study regions and time periods analyzed in different studies are responsible for those discrepancies in Arctic CF trends. No significant trend was found in CMIP6 LWP/IWP during the 14-year study period either, while the inter-annual variations are large for both parameters.

4 Summary and discussion

Arctic Basin surface radiation budget, clouds and the cloud radiative effects (CREs) in the atmospheric model intercomparison project (AMIP) experiments of 22 CMIP6 models have been evaluated against satellite observations for 2001–2014. The main conclusions are summarized below.

(1) Most of the 22 CMIP6 models show smaller annual net shortwave (SW) radiation than CERES-EBAF. The multi-model mean net longwave (LW) radiation in CMIP6 models is much larger than CERES-EBAF during spring and summer. The mean bias and the root-mean-square error (RMSE) of annual averaged net LW between multi-model mean and CERES-EBAF are 8.4 W/m^2 and 8.6 W/m^2, larger than those for net SW (–5.3 W/m^2 and 5.5 W/m^2). The underestimation of SW radiation and overestimation of LW radiation in CMIP6 are partially canceled each other out, resulting in a 3.1 W/m^2 bias in annual mean net radiation compared to CERES-EBAF. The spatial variations of SW, LW and net radiation within the Arctic Basin are small in the

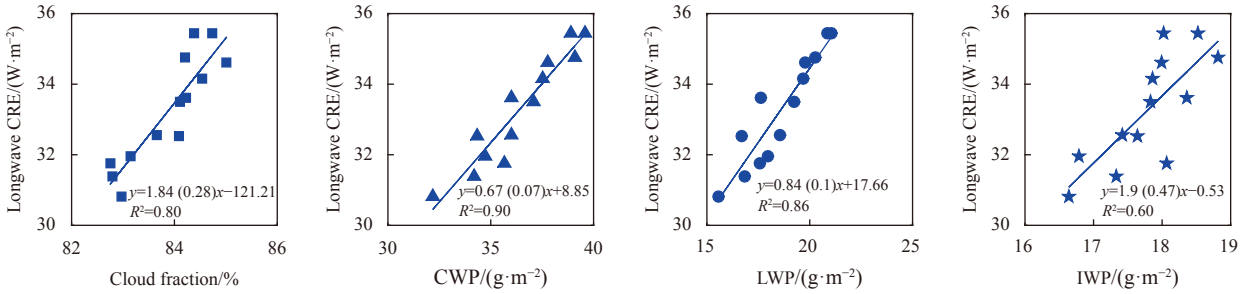


Fig. 14. Scatter plots of Arctic Basin cloud properties and cloud CREs in winter (DJF) during 2001–2014 based on CMIP6 models. The dots are values of CREs/cloud properties for 14 years. Regression lines are the linear fittings of these dots with the uncertainty of the slope in parentheses. The determination coefficients (R^2) of fitting lines are also shown.

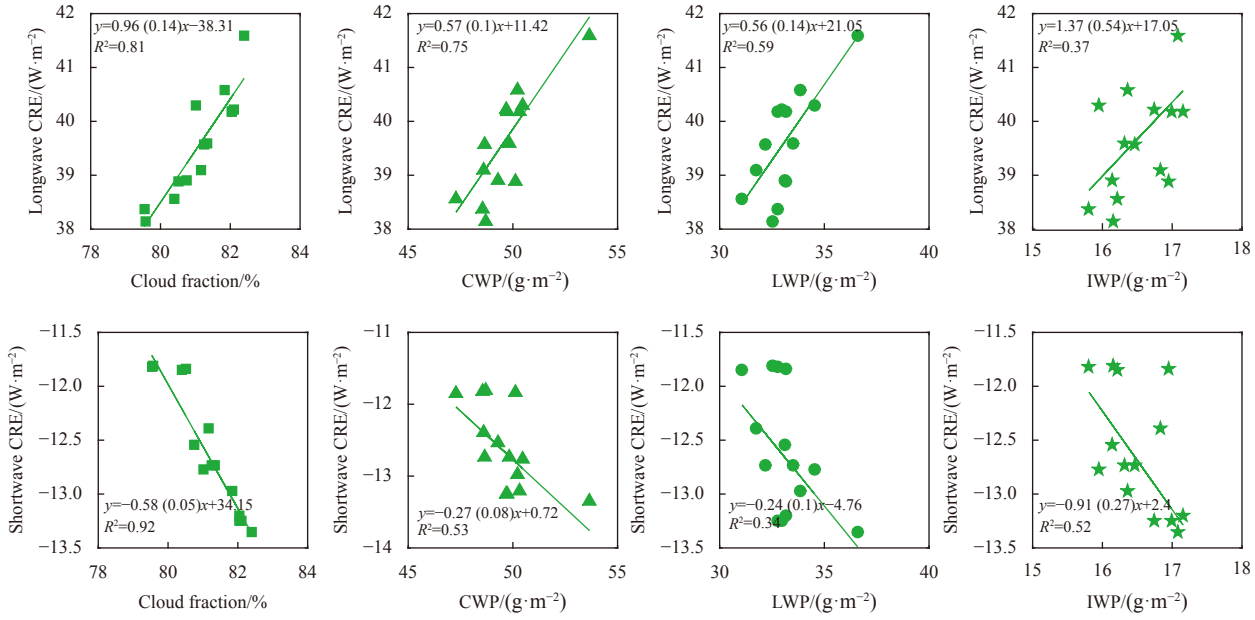


Fig. 15. Scatter plots of Arctic Basin cloud properties and cloud CREs in spring (MAM) during 2001–2014 based on CMIP6 models. The dots are values of CREs/cloud properties for 14 years. Regression lines are the linear fittings of these dots with the uncertainty of the slope in parentheses. The determination coefficients (R^2) of fitting lines are also shown.

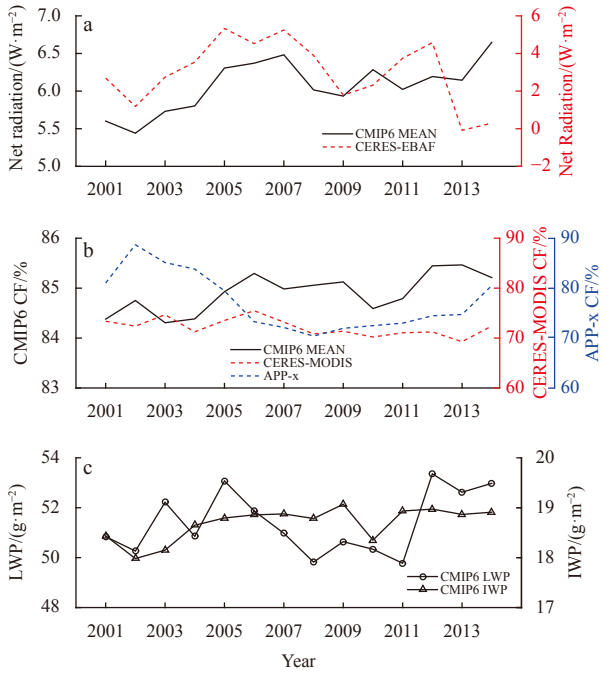


Fig. 16. Arctic Basin annual mean surface net radiative flux (a), CF (b), and CWPs (c) from available observations and the CMIP6 models over 2001–2014.

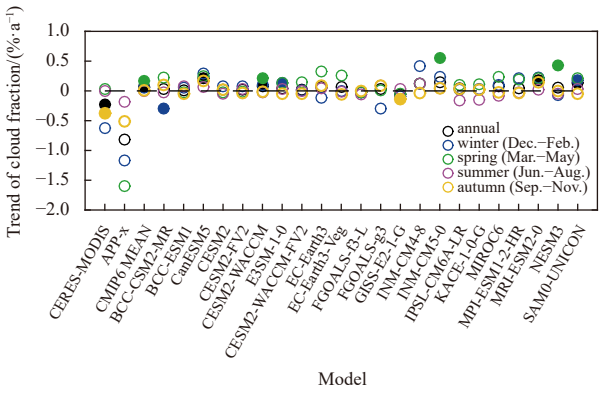


Fig. 17. Linear trends of the annual and seasonal mean Arctic Basin CFs derived from CERES-MODIS, APP-x and CMIP6 model output. The solid circles indicate the trends passing 95% Mann-Kendall significance test.

CMIP6 multi-model mean result. Simulated annual mean net surface radiation fluxes are positive in most models except for three models (EC-Earth3, EC-Earth3-Veg and FGOALS-g3).

(2) Generally, Arctic Basin cloud fraction (CF) in CMIP6 models shows consistent spatial patterns with the observations from CloudSat-CALIPSO, CERES-MODIS, and APP-x during the period (2007–2010) when all these data were available, with lower fraction in the Pacific sector than in the Atlantic sector. During 2001–2014, the multi-model mean annual CF in CMIP6 is closer to APP-x than CERES-MODIS, but the seasonal variation is similar to CERES-MODIS. The spread of CF among the CMIP6 models is much smaller than in CMIP5 if excluding the extremely low CF in FGOALS-g3. The seasonal cycles of cloud liquid water path (LWP) and ice water path (IWP) present large inter-model spreads, which are possibly resulted from the discrepancies of cloud microphysical parameterizations.

(3) Annually, net surface cloud radiative effect (CRE) in the Arctic Basin is positive. SW CRE is negative all year round, while LW CRE keeps positive except for summer months. The warming effects of CF, CWP and LWP on net LW are prominent in winter, while these effects are also significant for CF and CWP in spring. The cooling effect of CF on net SW is prominent in spring. The LW warming effect from CF in winter is also detected in CERES cloud and radiation observations.

(4) During 2001–2014, modeled net surface radiation within the Arctic Basin is well correlated with CERES-EBAF observation before the year 2008. Spring CF increases significantly in CMIP6 multi-model mean, which is in agreement with previous work based on AVHRR longer-term observations. The inter-annual variability of CF in CMIP6 models differs greatly from observations. Cloud LWP and IWP in CMIP6 models show great inter-annual variation but no obvious trend during the 14 years.

The model-observation discrepancies of Arctic cloud properties and surface radiation budget may have several sources. Passive remote sensing like MODIS has its challenges due to the poor thermal and visible contrast between clouds and the underlying snow and ice surface (especially at nighttime), small radiances from the cold polar atmosphere, and temperature inversions in the lower troposphere of polar regions (Liu et al., 2010). The spatial interpolation of satellite tracks may introduce errors in the gridded products in CERES-MODIS, APP-x, and CloudSat-CALIPSO. Moreover, the crude representation of surface albedo in the satellite product algorithms may lead to significant uncertainties in downwelling shortwave radiation retrievals, especially over the ice sheets and over sea ice in high latitudes.

More importantly, different cloud parameterization schemes used in different models lead to the large inter-model spreads in Arctic CF and surface radiation fluxes. In CMIP6 climate models, cloud cover is either parameterized through the relative humidity with some consideration of thermal stability effects (RH-based empirical or semi-empirical schemes) (e.g., BCC-CSM2-MR, FGOALS-g3, GISS-E2-1-G, NESM3), or determined by accounting for the sub-grid scale variability in both water content and temperature using PDF-based scheme (e.g., CESM2, E3SM-1-0, IPSL-CM6A-LR). As pointed out by previous studies, climate models cannot reproduce realistic strong inversions especially those in the polar region due to their insufficient vertical resolution (e.g., Kawai et al., 2019). In addition, five models (EC-Earth3, EC-Earch3-Veg, INM-CM4-8, INM-CM5-0, and KACE-1-0-G) take CF as a prognostic variable. The source and sink terms of the prognostic equation include boundary layer turbulence and large-scale condensation and evaporation. Thus the models' abilities of simulating cloud cover and CREs are also related to the different planetary boundary layer (PBL) schemes used in different models. Therefore, inter-model spreads and model-satellite observation differences are introduced by those problems.

Due to the short and incomplete observational records, as well as the limited COSP output of CMIP6 models, large uncertainties exist in the analyses of the Arctic surface radiation budget and the role clouds play. Surface cloud radiative forcing depends not only on the cloud macrophysical properties (e.g., cloud fraction), but also the microphysical properties. We suggest that future studies and model simulations should focus on better constraining physical processes related to cloud formation and cloud radiative feedback using more observational data sets.

Acknowledgements

We thank the climate modeling groups of CMIP6 for produ-

cing and making available their model output. All data used in this study are available online. The CMIP6 model results could be downloaded from https://pcmdi.llnl.gov/CMIP6/. Satellite observational products of cloud properties and surface radiation fluxes from CERES are available at http://ceres.larc.nasa.gov/. APP-x cloud fraction data can be downloaded via https://www.ncdc.noaa.gov/cdr/atmospheric/extended-avhrr-polar-pathfinder-app-x. Gridded cloud products of CloudSat-CALIPSO are downloaded from https://icdc.cen.uni-hamburg.de. We thank Kun Wu for the discussion on the cloud radiative effects in high latitudes.

References

Bodas-Salcedo A, Webb M J, Bony S, et al. 2011. COSP: Satellite simulation software for model assessment. Bulletin of the American Meteorological Society, 92(8): 1023–1043, doi: 10.1175/2011BAMS2856.1

Boeke R C, Taylor P C. 2016. Evaluation of the Arctic surface radiation budget in CMIP5 models. Journal of Geophysical Research: Atmospheres, 121(14): 8525–8548, doi: 10.1002/2016JD025099

Bogenschutz P A, Gettelman A, Hannay C, et al. 2018. The path to CAM6: Coupled simulations with CAM5.4 and CAM5.5. Geoscientific Model Development, 11(1): 235–255, doi: 10.5194/gmd-11-235-2018

Cao Jian, Wang Bin, Yang Y M, et al. 2018. The NUIST Earth System Model (NESM) version 3: Description and preliminary evaluation. Geoscientific Model Development, 11(7): 2975–2993, doi: 10.5194/gmd-11-2975-2018

Cesana G, Kay J E, Chepfer H, et al. 2012. Ubiquitous low level liquid-containing Arctic clouds: New observations and climate model constraints from CALIPSO-GOCCP. Geophysical Research Letters, 39(20): L20804, doi: 10.1029/2012GL053385

Cesana G, Storelvmo T. 2017. Improving climate projections by understanding how cloud phase affects radiation. Journal of Geophysical Research: Atmospheres, 22(8): 4594–4599, doi: 10.1002/2017JD026927

Christensen M W, Behrangi A, L'ecuyer T S, et al. 2016. Arctic observation and reanalysis integrated system: A new data product for validation and climate study. Bulletin of the American Meteorological Society, 97(6): 907–916, doi: 10.1175/BAMS-D-14-00273.1

Cohen J, Screen J A, Furtado J C, et al. 2014. Recent Arctic amplification and extreme mid-latitude weather. Nature Geoscience, 7(9): 627–637, doi: 10.1038/ngeo2234

Comiso J C, Hall D K. 2014. Climate trends in the Arctic as observed from space. Wiley Interdisciplinary Reviews: Climate Change, 5(3): 389–409, doi: 10.1002/wcc.277

Dong Xiquan, Xi Baike, Crosby K, et al. 2010. A 10 year climatology of Arctic cloud fraction and radiative forcing at Barrow, Alaska. Journal of Geophysical Research: Atmospheres, 115(D17): D17212, doi: 10.1029/2009JD013489

Dong Xiquan, Xi Baike, Qiu Shaoyue, et al. 2016. A radiation closure study of Arctic stratus cloud microphysical properties using the collocated satellite-surface data and Fu-Liou radiative transfer model. Journal of Geophysical Research: Atmospheres, 121(17): 10175–10198, doi: 10.1002/2016JD025255

Eastman R, Warren S G. 2010. Interannual variations of Arctic cloud types in relation to sea ice. Journal of Climate, 23(15): 4216–4232, doi: 10.1175/2010JCLI3492.1

English J M, Gettelman A, Henderson G R. 2015. Arctic radiative fluxes: Present-day biases and future projections in CMIP5 models. Journal of Climate, 28(15): 6019–6038, doi: 10.1175/JCLI-D-14-00801.1

Eyring V, Bony S, Meehl G A, et al. 2016. Overview of the coupled model intercomparison project Phase 6 (CMIP6) experimental design and organization. Geoscientific Model Development, 9(5): 1937–1958, doi: 10.5194/gmd-9-1937-2016

Forbes R, Ahlgrimm M. 2012. Representing cloud and precipitation in the ECMWF global model. In: ECMWF Workshop on Parametrization of Clouds and Precipitation. Reading, UK: European Centre for Medium-Range Weather Forecasts

Fu Qiang, Liou K N. 1993. Parameterization of the radiative properties of cirrus clouds. Journal of the Atmospheric Sciences, 50(13): 2008–2025, doi: 10.1175/1520-0469(1993)050<2008:POTRPO>2.0.CO;2

Goosse H, Kay J E, Armour K C, et al. 2018. Quantifying climate feedbacks in polar regions. Nature Communications, 9: 1919, doi: 10.1038/s41467-018-04173-0

Guo Zhun, Zhou Tianjun. 2014. An improved diagnostic stratocumulus scheme based on estimated inversion strength and its performance in GAMIL2. Science China Earth Sciences, 57(11): 2637–2649, doi: 10.1007/s11430-014-4891-7

He Bian, Bao Qing, Wang Xiaocong, et al. 2019. CAS FGOALS-f3-L model datasets for CMIP6 historical atmospheric model intercomparison project simulation. Advances in Atmospheric Sciences, 36(8): 771–778, doi: 10.1007/s00376-019-9027-8

Hourdin F, Rio C, Grandpeix J Y, et al. 2020. LMDZ6A: The atmospheric component of the IPSL climate model with improved and better tuned physics. Journal of Advances in Modeling Earth Systems, 12(7): e2019MS001892, doi: 10.1029/2019MS001892

Huang Yiyi, Dong Xiquan, Bailey D A, et al. 2019. Thicker clouds and accelerated Arctic sea ice decline: The atmosphere-sea ice interactions in spring. Geophysical Research Letters, 46(12): 6980–6989, doi: 10.1029/2019GL082791

Huang Yiyi, Dong Xiquan, Xi Baike, et al. 2017a. Quantifying the uncertainties of reanalyzed Arctic cloud and radiation properties using satellite surface observations. Journal of Climate, 30(19): 8007–8029, doi: 10.1175/JCLI-D-16-0722.1

Huang Yiyi, Dong Xiquan, Xi Baike, et al. 2017b. The footprints of 16 year trends of Arctic springtime cloud and radiation properties on September Sea Ice retreat. Journal of Geophysical Research: Atmospheres, 122(4): 2179–2193, doi: 10.1002/2016JD026020

Intergovernmental Panel on Climate Change (IPCC). 2014. Climate Change 2013: The Physical Science Basis. Contribution of Working Group I to the Fifth Assessment Report of the Intergovernmental Panel on Climate Change. Cambridge, UK: Cambridge University Press

Jun S Y, Ho C H, Jeong J H, et al. 2016. Recent changes in winter Arctic clouds and their relationships with sea ice and atmospheric conditions. Tellus A: Dynamic Meteorology and Oceanography, 68(1): 29130, doi: 10.3402/tellusa.v68.29130

Kapsch M L, Graversen R G, Tjernström M. 2013. Springtime atmospheric energy transport and the control of arctic summer sea-ice extent. Nature Climate Change, 3(8): 744–748, doi: 10.1038/nclimate1884

Karlsson K G, Anttila K, Trentmann J, et al. 2017. CLARA-A2: CM SAF cLoud, Albedo and Surface Radiation Dataset from AVHRR data-Edition 2. Offenbach: Satellite Application Facility on Climate Monitoring, doi: 10.5676/EUM_SAF_CM/CLARA_AVHRR/V002

Kato S, Rose F G, Rutan D A, et al. 2018. Surface irradiances of edition 4.0 Clouds and the Earth's Radiant Energy System (CERES) Energy Balanced and Filled (EBAF) data product. Journal of Climate, 31(11): 4501–4527, doi: 10.1175/JCLI-D-17-0523.1

Kawai H, Yukimoto S, Koshiro T, et al. 2019. Significant improvement of cloud representation in the global climate model MRI-ESM2. Geoscientific Model Development, 12(7): 2875–2897, doi: 10.5194/gmd-12-2875-2019

Kay J E, Gettelman A. 2009. Cloud influence on and response to seasonal Arctic sea ice loss. Journal of Geophysical Research: Atmospheres, 114(D18): D18204, doi: 10.1029/2009JD011773

Kay J E, L'Ecuyer T. 2013. Observational constraints on Arctic Ocean clouds and radiative fluxes during the early 21st century. Journal of Geophysical Research: Atmospheres, 118(13): 7219–7236, doi: 10.1002/jgrd.50489

Kelley M, Schmidt G A, Nazarenko L, et al. 2020. GISS-E2.1: Configurations and climatology. Journal of Advances in Modeling Earth Systems, 12(8): e2019MS002025

Key J E, Wang Xuanji, Liu Yinghui. 2014. NOAA Climate Data Record

of AVHRR Polar Pathfinder Extended (APP-X): Version 1, Revision 1. Asheville, NC, USA: NOAA National Climate Data Center

Key J E, Wang Xuanji, Liu Yinghui, et al. 2016. The AVHRR polar pathfinder climate data records. Remote Sensing, 8(3): 167, doi: 10.3390/rs8030167

Lee H J, Kwon M O, Yeh S W, et al. 2017. Impact of poleward moisture transport from the North Pacific on the acceleration of sea ice loss in the Arctic since 2002. Journal of Climate, 30(17): 6757–6769, doi: 10.1175/JCLI-D-16-0461.1

Lenaerts J T M, Van Tricht K, Lhermitte S, et al. 2017. Polar clouds and radiation in satellite observations, reanalyses, and climate models. Geophysical Research Letters, 44(7): 3355–3364, doi: 10.1002/2016GL072242

Letterly A, Key J, Liu Yinghui. 2016. The influence of winter cloud on summer sea ice in the Arctic, 1983–2013. Journal of Geophysical Research: Atmospheres, 121(5): 2178–2187, doi: 10.1002/2015JD024316

Li Jiming, Yi Yuhong, Minnis P, et al. 2011. Radiative effect differences between multi-layered and single-layer clouds derived from CERES, CALIPSO, and CloudSat data. Journal of Quantitative Spectroscopy and Radiative Transfer, 112(2): 361–375, doi: 10.1016/j.jqsrt.2010.10.006

Liu Yinghui, Ackerman S A, Maddux B C, et al. 2010. Errors in cloud detection over the Arctic using a satellite imager and implications for observing feedback mechanisms. Journal of Climate, 23(7): 1894–1907, doi: 10.1175/2009JCLI3386.1

Liu Yinghui, Key J R. 2014. Less winter cloud aids summer 2013 Arctic sea ice return from 2012 minimum. Environmental Research Letters, 9(4): 044002, doi: 10.1088/1748-9326/9/4/044002

Liu Yinghui, Key J R, Liu Zhengyu, et al. 2012. A cloudier Arctic expected with diminishing sea ice. Geophysical Research Letters, 39(5): L05705, doi: 10.1029/2012GL051251

Liu Yinghui, Key J R, Wang Xuanji. 2008. The influence of changes in cloud cover on recent surface temperature trends in the Arctic. Journal of Climate, 21(4): 705–715, doi: 10.1175/2007JCLI1681.1

Loeb N G, Doelling D R, Wang Hailan, et al. 2018. Clouds and the Earth's radiant energy system (CERES) energy balanced and filled (EBAF) top-of-atmosphere (TOA) edition-4.0 data product. Journal of Climate, 31(2): 895–918, doi: 10.1175/JCLI-D-17-0208.1

Mace G G, Benson S. 2008. The vertical structure of cloud occurrence and radiative forcing at the SGP ARM site as revealed by 8 years of continuous data. Journal of Climate, 21(11): 2591–2610, doi: 10.1175/2007JCLI1987.1

Mace G G, Zhang Qiuqing, Vaughan M, et al. 2009. A description of hydrometeor layer occurrence statistics derived from the first year of merged Cloudsat and CALIPSO data. Journal of Geophysical Research: Atmospheres, 114(D8): D00A26, doi: 10.1029/2007JD009755

Marchand R, Mace G G, Ackerman T, et al. 2008. Hydrometeor detection using Cloudsat — An earth-orbiting 94-GHz cloud radar. Journal of Atmospheric and Oceanic Technology, 25(4): 519–533, doi: 10.1175/2007jtecha1006.1

Matus A V, L'Ecuyer T S. 2017. The role of cloud phase in Earth's radiation budget. Journal of Geophysical Research: Atmospheres, 122(5): 2559–2578, doi: 10.1002/2016JD025951

McAvaney B J, Le Treut H. 2003. CFMIP: The cloud feedback intercomparison project. CLIVAR Exchanges, United Kingdom: International CLIVAR Project Office

Minnis P, Sun-Mack S, Young D F, et al. 2011. CERES Edition-2 cloud property retrievals using TRMM VIRS and terra and aqua MODIS data—Part I: Algorithms. IEEE Transactions on Geoscience and Remote Sensing, 49(11): 4374–4400, doi: 10.1109/TGRS.2011.2144601

Ogura T, Shiogama H, Watanabe M, et al. 2017. Effectiveness and limitations of parameter tuning in reducing biases of top-of-atmosphere radiation and clouds in MIROC version 5. Geoscientific Model Development, 10(12): 4647–4664, doi: 10.5194/gmd-10-4647-2017

Park S, Baek E H, Kim B M, et al. 2017. Impact of detrained cumulus on climate simulated by the community atmosphere model version 5 with a unified convection scheme. Journal of Advances in Modeling Earth Systems, 9(2): 1399–1411, doi: 10.1002/2016MS000877

Park S, Shin J, Kim S, et al. 2019. Global climate simulated by the Seoul National University Atmosphere Model version 0 with a unified convection scheme (SAM0-UNICON). Journal of Climate, 32(10): 2917–2949, doi: 10.1175/JCLI-D-18-0796.1

Perovich D K, Light B, Eicken H, et al. 2007. Increasing solar heating of the Arctic Ocean and adjacent seas, 1979–2005: Attribution and role in the ice-albedo feedback. Geophysical Research Letters, 34(19): L19505, doi: 10.1029/2007GL031480

Perovich D K, Moritz R C, Weatherly J. 1999. SHEBA: The surface heat budget of the Arctic Ocean. EOS, Transactions, American Geophysical Union, 80(41): 481–486

Platnick S, King M D, Ackerman S A, et al. 2003. The MODIS cloud products: Algorithms and examples from Terra. IEEE Transactions on Geoscience and Remote Sensing, 41(2): 459–473, doi: 10.1109/TGRS.2002.808301

Qu Xin, Hall A, Klein S A, et al. 2014. On the spread of changes in marine low cloud cover in climate model simulations of the 21st century. Climate Dynamics, 42(9-10): 2603–2626, doi: 10.1007/s00382-013-1945-z

Rasch P J, Xie S, Ma P L, et al. 2019. An overview of the atmospheric component of the Energy Exascale Earth System Model. Journal of Advances in Modeling Earth Systems, 11(8): 2377–2411, doi: 10.1029/2019MS001629

Riihelä A, Key J R, Meirink J F, et al. 2017. An intercomparison and validation of satellite-based surface radiative energy flux estimates over the Arctic. Journal of Geophysical Research: Atmospheres, 122(9): 4829–4848, doi: 10.1002/2016JD026443

Serreze M C, Barry R G. 2011. Processes and impacts of Arctic amplification: A research synthesis. Global and Planetary Change, 77(1-2): 85–96, doi: 10.1016/j.gloplacha.2011.03.004

Shupe M D, Matrosov S Y, Uttal T. 2006. Arctic mixed-phase cloud properties derived from surface-based sensors at SHEBA. Journal of the Atmospheric Sciences, 63(2): 697–711, doi: 10.1175/JAS3659.1

Shupe M D, Persson P O G, Brooks I M, et al. 2013. Cloud and boundary layer interactions over the Arctic sea ice in late summer. Atmospheric Chemistry and Physics, 13(18): 9379–9399, doi: 10.5194/acp-13-9379-2013

Slater A G. 2016. Surface solar radiation in North America: A comparison of observations, reanalyses, satellite, and derived products. Journal of Hydrometeorology, 17(1): 401–420, doi: 10.1175/JHM-D-15-0087.1

Spangenberg D A, Trepte Q, Minnis P, et al. 2004. Daytime cloud property retrievals over the Arctic from multispectral MODIS data. In: 13th AMS Conference on Satellite Oceanography and Meteorology. Norfolk, VA: Bulletin of the American Meteorological Society

Stevens B, Giorgetta M, Esch M, et al. 2013. Atmospheric component of the MPI-M Earth system model: ECHAM6. Journal of Advances in Modeling Earth Systems, 5(2): 146–172, doi: 10.1002/jame.20015

Stokes G M, Schwartz S E. 1994. The Atmospheric Radiation Measurement (ARM) Program: Programmatic background and design of the cloud and radiation test bed. Bulletin of the American Meteorological Society, 75(7): 1201–1222, doi: 10.1175/1520-0477(1994)075<1201:TARMPP>2.0.CO;2

Stubenrauch C J, Rossow W B, Kinne S, et al. 2013. Assessment of global cloud datasets from satellites: Project and database initiated by the GEWEX Radiation Panel. Bulletin of the American Meteorological Society, 94(7): 1031–1049, doi: 10.1175/BAMS-D-12-00117.1

Tatebe H, Ogura T, Nitta T, et al. 2019. Description and basic evaluation of simulated mean state, internal variability, and climate sensitivity in MIROC6. Geoscientific Model Development, 12(7): 2727–2765, doi: 10.5194/gmd-12-2727-2019

Taylor P C, Boeke R C, Li Ying, et al. 2019. Arctic cloud annual cycle biases in climate models. Atmospheric Chemistry and Physics,

19(13): 8759–8782, doi: 10.5194/acp-19-8759-2019
Tiedtke M. 1993. Representation of clouds in large-scale models. Monthly Weather Review, 121(11): 3040–3061, doi: 10.1175/1520-0493(1993)121<3040:ROCILS>2.0.CO;2
Tjernström M, Leck C, Birch C E, et al. 2014. The arctic summer cloud ocean study (ASCOS): Overview and experimental design. Atmospheric Chemistry and Physics, 14(6): 2823–2869, doi: 10.5194/acp-14-2823-2014
Trepte Q Z, Minnis P, Sun-Mack S, et al. 2019. Global cloud detection for CERES Edition 4 using Terra and Aqua MODIS data. IEEE Transactions on Geoscience and Remote Sensing, 57(11): 9410–9449, doi: 10.1109/TGRS.2019.2926620
Uttal T, Curry J A, McPhee M G, et al. 2002. Surface heat budget of the Arctic Ocean. Bulletin of the American Meteorological Society, 83(2): 255–276, doi: 10.1175/1520-0477(2002)083<0255:SHBOTA>2.3.CO;2
Van Tricht K, Lhermitte S, Lenaerts J T M, et al. 2016. Clouds enhance Greenland ice sheet meltwater runoff. Nature Communications, 7: 10266, doi: 10.1038/ncomms10266
Vaughan M A, Powell K A, Winker D M, et al. 2009. Fully automated detection of cloud and aerosol layers in the CALIPSO lidar measurements. Journal of Atmospheric and Oceanic Technology, 26(10): 2034–2050, doi: 10.1175/2009jtecha1228.1
Verlinde J, Zak B D, Shupe M D, et al. 2016. The ARM north slope of Alaska (NSA) sites. Meteorological Monographs, 57: 8.1–8.13, doi: 10.1175/AMSMONOGRAPHS-D-15-0023.1
Von Salzen K, Scinocca J F, McFarlane N A, et al. 2013. The Canadian fourth generation atmospheric global climate model (CanAM4). Part I: Representation of physical processes. Atmosphere-Ocean, 51(1): 104–125, doi: 10.1080/07055900.2012.755610
Walsh J E. 2014. Intensified warming of the Arctic: Causes and impacts on middle latitudes. Global Planetary Change, 117: 52–63, doi: 10.1016/j.gloplacha.2014.03.003
Walters D, Baran A J, Boutle I, et al. 2019. The met office unified model global atmosphere 7.0/7.1 and JULES global land 7.0 configurations. Geoscientific Model Development, 12(5): 1909–1963, doi: 10.5194/gmd-12-1909-2019
Wang Xuanji, Key J R. 2005a. Arctic surface, cloud, and radiation properties based on the AVHRR polar pathfinder dataset. Part I: Spatial and temporal characteristics. Journal of Climate, 18(14): 2558–2574, doi: 10.1175/JCLI3438.1
Wang Xuanji, Key J R. 2005b. Arctic surface, cloud, and radiation properties based on the AVHRR polar pathfinder dataset. Part II: Recent trends. Journal of Climate, 18(14): 2575–2593, doi: 10.1175/JCLI3439.1
Wang Xiaocong, Liu Yimin, Bao Qing, et al. 2015. Comparisons of GCM cloud cover parameterizations with cloud-resolving model explicit simulations. Science China: Earth Sciences, 58(4): 604–614, doi: 10.1007/s11430-014-4989-y
Wang Yunhe, Yuan Xiaojun, Bi Haibo, et al. 2019. The contributions of winter cloud anomalies in 2011 to the summer sea-ice rebound in 2012 in the Antarctic. Journal of Geophysical Research: Atmospheres, 124(6): 3435–3447, doi: 10.1029/2018JD029435
Webb M J, Andrews T, Bodas-Salcedo A, et al. 2017. The cloud feedback model intercomparison project (CFMIP) contribution to CMIP6. Geoscientific Model Development, 10(1): 359–384, doi: 10.5194/gmd-10-359-2017
Wei Jianfen, Zhang Xiangdong, Wang Zhaomin. 2019. Reexamination of Fram Strait sea ice export and its role in recently accelerated Arctic sea ice retreat. Climate Dynamics, 53(3–4): 1823–1841, doi: 10.1007/s00382-019-04741-0
Wendisch M, Macke A, Ehrlich A, et al. 2019. The Arctic cloud puzzle: Using ACLOUD/PASCAL multiplatform observations to unravel the role of clouds and aerosol particles in arctic amplification. Bulletin of the American Meteorological Society, 100(5): 841–871, doi: 10.1175/BAMS-D-18-0072.1
Wielicki B A, Barkstrom B R, Baum B A, et al. 1998. Clouds and the Earth's Radiant Energy Sys-tem (CERES): Algorithm overview. IEEE Transactions on Geoscience and Remote Sensing, 36(4): 1127–1141, doi: 10.1109/36.701020
Wielicki B A, Barkstrom B R, Harrison E F, et al. 1996. Clouds and the Earth's Radiant Energy System (CERES): an earth observing system experiment. Bulletin of the American Meteorological Society, 77(5): 853–868, doi: 10.1175/1520-0477(1996)077<0853:CATERE>2.0.CO;2
Wilson D R, Bushell A C, Kerr-Munslow A M, et al. 2008. PC2: A prognostic cloud fraction and condensation scheme. II: Climate model simulations. Quarterly Journal of the Royal Meteorological Society, 134(637): 2109–2125, doi: 10.1002/qj.332
Wu Tongwen, Lu Yixiong, Fang Yongjie, et al. 2019. The Beijing climate center climate system model (BCC-CSM): The main progress from CMIP5 to CMIP6. Geoscientific Model Development, 12(4): 1573–1600, doi: 10.5194/gmd-12-1573-2019
Xu Kuanman, Randall D A. 1996. A semiempirical cloudiness parameterization for use in climate models. Journal of the Atmospheric Sciences, 53(21): 3084–3102, doi: 10.1175/1520-0469(1996)053<3084:ASCPFU>2.0.CO;2
Yu Wei, Doutriaux M, Sèze G, et al. 1996. A methodology study of the validation of clouds in GCMs using ISCCP satellite observations. Climate Dynamics, 12(6): 389–401, doi: 10.1007/bf00211685
Yu Yueyue, Taylor P C, Cai Ming. 2019. Seasonal variations of arctic low-level clouds and its linkage to sea ice seasonal variations. Journal of Geophysical Research: Atmospheres, 124(22): 12206–12226, doi: 10.1029/2019JD031014
Zhang Xiaotong, Liang Shunlin, Wild M, et al. 2015. Analysis of surface incident shortwave radiation from four satellite products. Remote Sensing of Environment, 165: 186–202, doi: 10.1016/j.rse.2015.05.015
Zhang Yuying, Xie Shaocheng, Lin Wuyin, et al. 2019. Evaluation of clouds in version 1 of the E3SM atmosphere model with satellite simulators. Journal of Advances in Modeling Earth Systems, 11(5): 1253–1268, doi: 10.1029/2018MS001562